Highlights

We assess mechanisms regulating evapotranspiration (*E*) in Amazonia and cerrado.

Groundwater and deep root uptake can both sustain *E* during the dry season.

Canopy stomatal conductance regulates *E* even at sites with little water limitation.

Models capturing observed patterns in *E* may still poorly represent these mechanisms.

Models developments should focus on improved biological controls on *E*.

Title: Mechanisms of water supply and vegetation demand govern the seasonality and magnitude of evapotranspiration in Amazonia and Cerrado

Authors: Bradley O. Christoffersen[a,b 1]*, Natalia Restrepo-Coupe[a,c], M Altaf Arain[d], Ian T. Baker[e], Bruno P. Cestaro[f], Phillippe Ciais[g], Joshua B. Fisher[h], David Galbraith[i j], Xiaodan Guan[k], Lindsey Gulden[k l], Bart van den Hurk[m], Kazuhito Ichii[n], Hewlley Imbuzeiro[o], Atul Jain[p], Naomi Levine[q], Gonzalo Miguez-Macho[r], Ben Poulter[s], Debora R Roberti[t], Koichi Sakaguchi[b], Alok Sahoo[u], Kevin Schaefer[v], Mingjie Shi[k], Hans Verbeeck[w], Zong-Liang Yang[k], Alessandro C. Araújo[x], Bart Kruijt[y], Antonio O. Manzi[z], Humberto R. da Rocha[f], Celso von Randow[aa], Michel N. Muza[bb], Jordan Borak[cc], Marcos H. Costa[o], Luis Gustavo G. de Gonçalves[bb cc], Xubin Zeng[b], and Scott R. Saleska[a]

a. Department of Ecology and Evolutionary Biology, University of Arizona, Tucson, AZ, USA
b. Department of Atmospheric Sciences, University of Arizona, Tucson, AZ, USA
c. Plant Functional Biology and Climate Change Cluster, University of Technology, Sydney, Australia
d. School of Geography and Earth Sciences, McMaster University, Hamilton, ON, Canada
e. Atmospheric Science Department, Colorado State University, Fort Collins, CO, USA
f. Departamento de Ciências Atmosfericas, IAG, Universidade de São Paulo, São Paulo, Brazil
g. LSCE CEA-CNRS-UVSQ, Orme des Merisiers, F-91191 Gif-sur-Yvette, France
h. Jet Propulsion Laboratory, California Institute of Technology, Pasadena, CA, USA
i. Environmental Change Institute, School of Geography and the Environment, University of Oxford, Oxford, OX1 3QY, UK
j. School of Geography, University of Leeds, Leeds, UK
k. Center for Integrated Earth System Science, Department of Geological Sciences, The University of Texas at Austin, Austin, TX, USA
l. ExxonMobil Upstream Research Company, Houston Texas, USA
m. Royal Netherlands Meteorological Institute (KNMI), De Bilt, Netherlands
n. Faculty of Symbiotic Systems Science, Fukushima University, Japan
o. Dep. Agricultural Engineering, Federal University of Viçosa, Viçosa, MG, Brazil
p. Department of Atmospheric Sciences, University of Illinois at Urbana-Champaign, Urbana, IL, USA
q. Department of Organismic and Evolutionary Biology, Harvard University, Cambridge, MA, USA
r. Physics Faculty, Universidade de Santiago de Compostela, Santiago de Compostela, Galicia, Spain
s. Swiss Federal Research Institute WSL, Dynamic Macroecology, Birmensdorf, Switzerland
t. Dept of Physics, Federal University of Santa Maria, Santa Maria, RS, Brazil
u. Center for Research on Environment and Water, IGES, Calverton, Maryland, USA
v. National Snow and Ice Data Center, Cooperative Institute for Research in Environmental Sciences, University of Colorado at Boulder, Boulder, CO 80309, USA
w. Laboratory of Plant Ecology, Ghent University, Ghent, Belgium
x. Embrapa Amazônia Oriental, Belém, PA, Brazil
y. Wageningen University & Research Center, Wageningen, Netherlands
z. Instituto Nacional de Pesquisas da Amazônia (INPA), Manaus, AM, Brazil
aa. Centro de Ciência do Sistema Terrestre (CCST), Instituto Nacional de Pesquisas Espaciais

(INPE), Cachoeira Paulista, SP, Brazil
bb. Earth System Science Interdisciplinary Center, University of Maryland, College Park; Hydrological Sciences Laboratory, NASA Goddard Space Flight Center
cc. Centro de Previsão de Tempo e Estudos Climáticos (CPTEC), Instituto Nacional de Pesquisas Espaciais (INPE),Cachoeira Paulista, SP, Brazil

* Corresponding author: Tel. + 1 (520) 626-5838; Fax + 1 (520) 621-9190; Email bradleychristo@gmail.com
1. Present address: School of GeoSciences, Crew Building, King's Buildings, University of Edinburgh, Edinburgh, EH9 3JN UK

Abstract

Evapotranspiration (*E*) in the Amazon connects forest function and regional climate via its role in precipitation recycling. However, the mechanisms regulating water supply to vegetation and its demand for water remain poorly understood, especially during periods of seasonal water deficits. In this study, we address two main questions: First, how do mechanisms of water supply (indicated by rooting depth and groundwater) and vegetation water demand (indicated by stomatal conductance and intrinsic water use efficiency) control evapotranspiration (*E*) along broad gradients of climate and vegetation from equatorial Amazonia to Cerrado, and second, how do these inferred mechanisms of supply and demand compare to those employed by a suite of ecosystem models? We used a network of eddy covariance towers in Brazil coupled with ancillary measurements to address these questions. With respect to the magnitude and seasonality of *E*, models have much improved in equatorial tropical forests by eliminating most dry season water limitation, diverge in performance in transitional forests where seasonal water deficits are greater, and mostly capture the observed seasonal depressions in *E* at Cerrado. However, many models depended universally on either deep roots or groundwater to mitigate dry season water deficits, the relative importance of which we found does not vary as a simple function of climate or vegetation. In addition, canopy stomatal conductance (g_s) regulates dry season vegetation demand for water at all except the wettest sites even as the seasonal cycle of *E* follows that of net radiation. In contrast, some models simulated no seasonality in g_s, even while matching the observed seasonal cycle of *E*. We suggest that canopy dynamics mediated by leaf phenology may play a significant role in such seasonality, a process poorly represented in models. Model bias in g_s and *E*, in turn, was related to biases arising from the simulated light response (gross primary productivity, *GPP*) or the intrinsic water use efficiency of photosynthesis (*iWUE*). We identified deficiencies in models which would not otherwise be apparent based on a simple comparison of simulated and observed rates of *E*. While some deficiencies can be remedied by parameter tuning, in most models they highlight the need for continued process development of belowground hydrology and in particular, the biological processes of root dynamics and leaf phenology, which via their controls on *E*, mediate vegetation-climate feedbacks in the tropics.

Keywords: tropical forest; evapotranspiration; deep roots; groundwater; canopy stomatal conductance; intrinsic water use efficiency

1. Introduction

Evapotranspiration (*E*) in the Amazon is the dominant connection between forest function and regional climate, primarily through its role in precipitation recycling (Victoria et al., 1991; Eltahir and Bras, 1994). Global circulation model (GCM) studies which simulate the effects of deforestation have shown a reduction of rainfall downwind (Walker et al., 1995), implying a coupling between the integrity of the Amazonian hydrometerological system and forest function. Such a coupling presents an opportunity for a positive feedback under climate change: should future rainfall in the Amazon decrease and forests downregulate metabolism via stomatal closure, rainfall reductions basin-wide could be exacerbated and further threaten forest integrity (Betts et al., 2004). Loss of a significant area of Amazon forest due to climate change, deforestation, or a combination of both can have further impacts globally due to hydrometerological teleconnections (Werth and Avissar, 2002) or carbon cycle feedbacks (Cox et al., 2000). However, much uncertainty remains surrounding modeling forest response to climate anomalies, due to both to model process differences/parameters or due to uncertainty in climate projections (Huntingford et al., 2008; Sitch et al., 2008; Galbraith et al., 2010; Poulter et al., 2010). This paper seeks to further investigate model process uncertainty by focusing on mechanisms controlling the seasonality and magnitude of *E* in the Amazon basin using a data-model intercomparison approach (de Gonçalves et al., 2013) .

Recent syntheses using data from eddy covariance measures of carbon, water, and energy exchange across Amazonia indicate a simple dependency of *E* on net radiation (R_n) for forest types ranging from seasonally wet to seasonally dry forests (Shuttleworth, 1988; Hasler and Avissar, 2007; Juarez et al., 2007; da Rocha et al., 2009; Fisher et al., 2009). However, this stands in stark contrast to many model predictions which instead have historically simulated an annual *E* cycle in phase with precipitation (*P*) (Shuttleworth, 1991; Bonan, 1998; Dickinson et al., 2006), suggesting that *E* is limited by water availability. Such a discrepancy between models and data indicates that knowledge of the mechanisms which regulate *E* remain poorly understood.

Uncertainty in ecosystem land surface models (LSMs) with respect to *E* fluxes can be

broadly grouped into those aspects relating to the supply of water to vegetation belowground and those involved in vegetation response to changes in water supply. In recent years, attention has been almost singularly focused on fixing the supply side of the problem, implementing deep soil and/or deep roots(Ichii et al., 2007; Baker et al., 2008; Grant et al., 2009; Harper et al., 2010; Verbeeck et al., 2011), root hydraulic redistribution (Lee et al., 2005), unconfined aquifers (Oleson et al., 2008; Fan and Miguez-Macho, 2010; Miguez-Macho and Fan, 2012), or changes to the numerical solution of the Richards equation for soil water fluxes (Zeng and Decker, 2009) to improve seasonal patterns of soil moisture and/or the seasonality of ecosystem metabolism in general. Despite the attention given to these ecohydrological mechanisms, little is known as to the relative contribution of soil physical versus biological mechanisms mediating supply.

On the other hand, control of the demand of water by vegetation in response to changes in water supply may be an equally important mechanism regulating the seasonality and magnitude of *E*. These have received comparatively less attention as a focus for model improvements. Canopy stomatal conductance and intrinsic water use efficiency (*iWUE*) are two key mechanisms controlling vegetation demand for water, respectively, in relation to atmospheric vapor pressure deficit (*D*) and ecosystem photosynthesis (*GPP*) arising from the 'photosynthesis-transpiration' compromise (Lloyd et al., 2002; Beer et al., 2009). The degree to which stomata regulate transpiration (E_t) independent of environmental conditions in the Amazon has been the topic of debate (Avissar and Werth, 2004; Costa et al., 2004). The conclusions of syntheses of eddy covariance measures of the seasonality of *E* in the Amazon have largely emphasized the secondary role of vegetation demand across a range of forest types (Costa et al., 2004; Juarez et al., 2007; da Rocha et al., 2009; Fisher et al., 2009), but recent work suggests that forests indeed exhibit varying degrees of control on the seasonal exchange of water in their canopies (Costa et al., 2010). Much of what is known about the functioning of stomata remains phenomenological and at the leaf-level, and attempts at forming a solid mechanistic basis of stomatal function have proven to be a challenge (Buckley, 2005; Peak and Mott, 2011).

The range of control points for *E* within the soil-plant-atmosphere continuum calls for a critical assessment of the 'state-of-art' mechanisms employed to predict *E* in ecosystem LSMs. We do so by addressing those involved in both the supply (belowground) and demand (aboveground) side. To be clear, the environment and vegetation both control aspects of supply and demand, the former being regulated by soil water and the root networks which exploit it (ecohydrological mechanisms) and the latter regulated both by the atmosphere (e.g., net radiation and vapor pressure deficit) and stomata (the latter representing ecophysiological mechanisms). This paper seeks to disentangle the relative role of abiotic and biotic controls on both supply and demand, and use these findings to evaluate modeled *E*.

We begin with a data-model comparison of the magnitude and seasonality of *E* from equatorial Amazonia to Cerrado and its first-order correlation with available energy (i.e., do models get the right answer?). This motivates a second-order analysis of supply and demand from observational and modeling perspectives (i.e., what are the mechanisms, and do models get the right answer for the right reasons?). With respect to water supply, we discriminate between the relative roles of capillary flux from groundwater (a physical mechanism; "bringing the water to the trees") and roots penetrating deep into the soil (a biological mechanism; "taking the trees to the water") in regulating *E* during seasonal water deficits. Next, with respect to vegetation demand for water, we assess how seasonal patterns of canopy stomatal conductance impact the seasonality of *E*, and how canopy intrinsic water use efficiency (*iWUE*; photosynthesis per unit evaporative potential of water through stomata) mediates the relationship between gross photosynthesis (*GPP*) and *E*. We use the available data to answer these questions while evaluating the suite of models with respect to these mechanisms of supply and demand. Finally, we derive a simple model benchmark which incorporates both right answer/right reason aspects of data-model intercomparison.

2. Materials and Methods

2.1. Site descriptions, grouping, and observational data

We selected five forest sites and one Cerrado site from a network of eddy covariance towers in Brazil called 'BrasilFlux' (Restrepo-Coupe et al., 2013), where measurements of climate and the turbulent exchange of water, carbon, and momentum at the ecosystem level had been made. General characteristics of the vegetation, climate, and soil at each site are given in Table 1. We grouped sites into three site groups based on similarities in the seasonality of precipitation (P) as well as net radiation (R_n) and latitude: equatorial evergreen forests (K34, K67, K83 sites), transitional semideciduous forests, which are semideciduous or ecotonal to Cerrado along the south-southeast margin of the Amazon (RJA, BAN sites), and Cerrado (savanna; PDG site), the southernmost site which is not within the Amazon basin (Fig. 1). The duration and strength of the dry season (defined as months where $P < 100$ mm) varied from short and moderate at the K34 evergreen tropical forest site to long and/or intense at the PDG Cerrado and BAN ecotonal sites (Table 1 and Fig. 1). In this paper, "equatorial forest" is not intended to be representative of Amazonian equatorial forests in general, since the sites presented occur mostly on highly weathered, relatively nutrient-poor soils, in contrast to western Amazonia where soils are shallow and more nutrient-rich which support forests with higher rates of vegetation productivity and turnover (Quesada et al., 2012). Our use of the term "transitional forest" differs somewhat from other studies (e.g., da Rocha et al. (2009)), as it includes both the semideciduous forest RJA site which is proximal to but not within the forest-Cerrado ecotone and the seasonally flooded BAN site which is within the forest-Cerrado ecotone and contains both cerradão (tall ~ 18-m trees) and cerrado sensu stricto (closed canopy of small 5m-tall trees interspersed with taller 7-10 m trees). The tower at the PDG Cerrado site is situated within a zone of cerrado sensu stricto (da Rocha et al., 2009). For additional site characteristics and ecosystem behavior, see Restrepo-Coupe et al. (2013) and references therein and da Rocha et al. (2009).

Table 1 also lists the temporal coverage and frequency of the climate measurements, eddy covariance data, and ancillary soil moisture data which are available at each site, in addition to the installation depths of soil moisture sensors. All eddy covariance data have been

processed according to a common protocol and are aggregated to an hourly timestep (Restrepo-Coupe et al., 2013). Soil moisture datasets were assimilated from various sources (see Table 1). The soil moisture data collection frequency ranged from near-continuous (half-hourly) to monthly and the monitored depths were variable across sites (data processing described in section 2.4 below and Appendix B in the Supplement).

2.2. Ecosystem model overview and selection

We used three to four years of climate measurements of short and long wave radiation, precipitation, air temperature, atmospheric pressure, humidity and horizontal wind speed to drive a suite of ecosystem models (23 variants in total) at each of the six sites according to a common spinup and initialization protocol. Participating models were part of the Large Scale Biosphere-Atmosphere Experiment in Amazonia Data Model Intercomparison Project (LBA-DMIP; de Gonçalves et al. (2013)). All models simulated ecosystem-level evapotranspiration (E) but used varying degrees of complexity for representing water supply and vegetation demand. 21 of the 23 model variants simulated a soil moisture store upon which vegetation draws for transpiration, but differed in the vertical resolution and depth of soil layers simulated (spanning 1.5 to 15 m), as well as the rooting depth used across sites. In most models, soil depth is synonymous with rooting depth. Five additional models simulated a groundwater store (also referred to as an unconfined aquifer) which could exchange water with the soil (both into and out). Table A2 in the supplementary information contains information on the models' soil depth, pedotransfer model and bottom boundary condition, in addition to the number of soil layers and rooting depths used across sites, and the associated model reference. On the demand side, 21 of the 23 model variants simulated canopy stomatal conductance (g_s), using one of four principal schemes to solve for g_s, E, and leaf-level photosynthesis (if simulated) given ambient incoming radiation, air temperature, and humidity: Jarvis-type (Jarvis, 1976) (four model variants), Leuning-type (Leuning et al., 1995) (four model variants), Ball-Woodrow-Berry-Collatz (Ball et al., 1987; Collatz et al., 1991) (11 model variants), or a constant ratio of internal to external leaf CO2 concentration (2 model variants). Table A3 in the supplementary

information gives the stomatal closure equations and parameter values for each model, and the associated model reference. For further information on participating models and details of model spinup and initialization procedures, see de Gonçalves et al. (2013) and references therein.

2.3. Atmospheric and vegetation controls on E

We conducted a first-order assessment of the realism of mechanisms regulating *E* in the models by comparing the degree to which energy available to evaporate water controlled *E*, in models versus in observations, during the dry season (defined as months where $P < 100$ mm). We quantified this control by regressing (for both models and observations) daily mean *LE* (W m^{-2}) on incoming energy and extracting the slope and R^2 values. The slope indicates the relative partitioning of available energy between *LE* and *H* (higher slopes mean more *LE*, i.e., a lower Bowen ratio, $\beta = H/LE$), while values of R^2 indicate the degree to which variability in available energy drives *LE*, as opposed to other variables (e.g., vapor pressure deficit, aerodynamic conductance, or soil water stress). R^2 values closer to 1 indicate that a large fraction of variation in *LE* can be explained by variation in available energy. We applied this approach uniformly across both simulations and eddy flux observations, pooling the data across sites by each site grouping (single site PDG in the case of Cerrado). We interpreted consistency between model-derived and observation-derived R^2 and slope values as one metric of realism of modeled controls on *E*.

For these regressions, we approximated available energy with the sum of latent and sensible heat ($LE + H$). Using $LE + H$ as an estimate of available energy instead of R_n is an approach recently adopted by a pan-tropical review of *LE* (Fisher et al., 2009) as an alternative to filtering out periods of poor energy budget closure (periods when $LE + H$ fall short of net radiation, R_n), which can reduce the number of daily replicates comprising a monthly mean (Costa et al., 2010). We recognize that such an approach inflates R^2 values and increases the slope, but absolute values are not the emphasis here. Rather, we sought a means by which to

assess site-site and model-data differences in the responses of *LE* to available energy in a way that was not confounded by varying degrees of energy budget closure in the observations. This allowed us to eliminate the possibility that differences in regression slopes or R^2 values across sites or between models and observations were due to the energy budget closure problem (since some sites' closure is better than others and all models have near-perfect closure).

2.4. Supply-side analysis of the seasonality of E*: coupling with soil moisture measurements*

All models presented were verified to have balanced the water budget; i.e., the following equation was always satisfied (de Gonçalves et al., 2013) to within 5 mm month^{-1}

$$P - E - Q_s - Q_{sb} + Q_{g\uparrow} = \frac{\Delta S_i + \Delta S_o + \Delta S_s}{\Delta t} \qquad (1)$$

where the left hand side represents the net water flux into the system in units of mm month^{-1} and the right hand side is the month-to-month differenced water storage of the system (Δt In months). P is precipitation, E is total evapotranspiration, Q_s is surface runoff, Q_{sb} is subsurface drainage, $Q_{g\uparrow}$ is vertical or lateral recharge to the soil from groundwater (positive from groundwater to unsaturated soil), ΔS_i is the change in canopy intercepted water, ΔS_o is the change in ponded surface open water, and ΔS_s is the change in total soil moisture. At the monthly timescale, ΔS_i and ΔS_o for all models were comparatively much smaller than ΔS_s.

We used a water budget approach to analyze supply-side mechanisms governing the seasonality of *E*. We combined precipitation and estimates of *E* with ancillary soil moisture measurements to estimate (as a residual) the seasonality of total runoff and groundwater recharge. This gave us all of the major components of the water budget for each site, and allowed us to infer the relative roles of upward capillary flux from groundwater and deep root uptake in sustaining dry season rates of *E*. These two mechanisms differentially impact both the magnitude and timing of the variability in total soil moisture; thus, quantifying the variability of

and timing of changes in ΔS_s provides a means for validating model mechanisms of water supply.

We used seasonal cycle estimates of E and month-month changes in stored soil moisture (ΔS_s), together with the seasonal cycle of precipitation (P) to estimate the seasonal cycle of total runoff (Q_t; positive means loss from the ecosystem), assuming a simple water balance model:

$$Q_t = P - E - \Delta S_s \quad (2)$$

We additionally assumed that month-to-month changes in stored canopy intercepted water were negligible. While we are unable to discriminate the partitioning of Q_t between surface runoff (Q_s) and subsurface drainage (Q_{sb}), we note that any Q_t occurring in the dry season will be dominated by subsurface drainage because surface soils are unsaturated. Most importantly, this approach also allows us to estimate the role of upward capillary flux or lateral transport from groundwater ($Q_{g\uparrow}$) during the dry season (inferred whenever $Q_t < 0$, or in other words, when the rate of soil moisture depletion is less than the rate of accumulating water deficit) as a mechanism for buffering dry season water deficits.

The seasonal cycle of P was estimated from the precipitation driver data, which was site-derived (de Gonçalves et al., 2013) . We estimated the seasonal cycle of E from hourly eddy covariance turbulent flux measurements by first making daily estimates from daylight hours, followed monthly E totals, and then averaging across years. Days with less than 80% data availability (Hasler and Avissar, 2007) and months with insufficient data for computing at least 7 daily totals were excluded. To derive modeled seasonal cycles of E, we used the entire model output, having determined that the seasonality of modeled E was not significantly impacted by removing model output hours during nighttime or periods of unavailable eddy flux observations of E.

To estimate the seasonal cycle of ΔS_s, we assimilated datasets of soil moisture measurements from various sources (Table 1). We estimated the month-to-month changes in

total soil moisture (ΔS_s) by aggregating to monthly means, integrating over depth, time differencing the monthly means, followed by averaging over replicate years. Where possible, we estimated the contribution to total ΔS_s of soil moisture below the measured domain (see Appendix B for methods), and found that at most sites and months, it was small (Supplement Fig. B4). The $Q_{g\uparrow}$ reported in Fig. 4 accounts for the additional variation in soil moisture beyond the measured depth up to the extrapolated depth reported in Table 1 for each site, except where extrapolation was not possible (PDG).

2.5. Demand-side analysis of the magnitude and seasonality of E

To provide a more rigorous assessment of the degree of potential dry season limitation of *E* by vegetation, we estimated seasonal variability in stand-level canopy stomatal conductance (g_s), using a top-down approach, similar to the inverted Penman-Monteith equation, but one which more closely approximates canopy stomatal conductance (as opposed to surface conductance) (Baldocchi et al., 1991). We applied the same top-down approach to extract canopy stomatal conductance from the models with hourly output (rather than using simulated canopy conductance directly) to make data-model intercomparison more straightforward. Models with daily output were excluded from these analyses because of the difficulty in estimating g_s from daily means. Exceptions are SiB3, SiBCASA and LEAFHYDRO models, which simulate a prognostic air space; canopy conductance from SiB3 and SiBCASA model output was used directly in lieu of the method described below.

The approach for estimating g_s is as follows: First, we estimated aerodynamic boundary layer resistance r_b (s m^{-1}):

$$r_b = \frac{\bar{u}}{u_*^2} \quad (3)$$

where $\bar{u}$ is the horizontal wind speed (m s^{-1}) and u_* is the friction velocity (m s^{-1}). Equation 3 follows Costa et al. (2010) and Hasler and Avissar (2007) who used it to estimate r_b (or its

inverse) at sites in central and southern Amazonia, many of which are the same sites reported here. While r_b can also be a function of measurement height, surface roughness and atmospheric stability, we kept a simple formulation based on the first-order $\bar{u}/u_*^2$ term because this avoids potential errors associated with second-order stability terms (Costa et al. 2010). We expect the biggest impact of not accounting for these higher-order terms to be in the magnitude of r_b estimated across sites, and so we focus on cross-site differences in the seasonality g_s (which depends on r_b; see Eq. 5 below), as opposed to its magnitude. We are still able, however, to compare the magnitude of g_s between models and data within a given site because we apply the same approach to estimate r_b and g_s in models and observations.

We then use r_b coupled with eddy covariance estimates of sensible heat flux (H; W m^{-2}) to estimate an aerodynamic canopy temperature T_v (^{o}C) by rearranging the gradient approximation for sensible heat flux (H):

$$T_v = \frac{r_b H}{c_p \rho_a} + T_a \quad (4)$$

where c_p is the specific heat capacity of dry air (J kg^{-1}), ρ_a is the atmospheric air density (kg m^{-3}), and T_a (^{o}C) is the atmospheric air temperature measured at the tower top. T_v is not necessarily leaf temperature, though the two are related. It is best understood as the temperature of the leaves and branches which contribute most to aerodynamic drag. Concurrent measurements of leaf temperature and an eddy covariance-estimated T_v at the K83 site show that the two are temporally correlated with each other but individual leaf temperatures can exceed T_v by as much as 8 ^{o}C under sunny conditions (Doughty and Goulden, 2008). Once T_v is known, we can estimate canopy stomatal conductance (Baldocchi et al., 1991):

$$g_s = \left[\frac{\rho_a (q_{sat}(T_v) - q_a)}{E_t} - r_b \right]^{-1} \quad (5)$$

where $q_{sat}(T_v)$ is the saturation specific humidity (kg kg^{-1}) at vegetation temperature T_v and q_a is

371 the ambient specific humidity (kg kg^{-1}), and E_t is the transpiration rate (kg m^{-2} s^{-1}).
372
373 We estimated E_t on a site-by-site basis as follows. First, we identified time periods when
374 canopy interception evaporation (E_i) was nonzero as predicted by the CLM3.5 model. Then,
375 assuming that these periods were a good proxy for times when the canopy was wet, we
376 removed these same periods from the *E* dataset prior to any averaging. For consistency, we
377 applied this same method on all models to estimate E_t from the models' *E* output (as opposed
378 to using the models' E_t output directly). While imperfect, this method ensured that E_t in
379 observations and models came from periods of identical environmental forcing. The method
380 used to estimate E_t is only suitable for analyzing its seasonality and relative magnitude across
381 models and observations, but not its absolute magnitude. This is because the method does not
382 equally sample the net radiation distribution, due to a bias towards cloud-free periods arising
383 from the need to exclude periods when the canopy was wet. For this reason, we did not
384 attempt to estimate the transpiration fraction of evapotranspiration, though it is likely a large
385 fraction for the forest sites (Jasechko et al., 2013).
386
387 The slope of leaf-level stomatal conductance versus photosynthesis is the parameter *m*
388 in the Ball-Woodrow-Berry-Collatz (BWBC) semi-empirical model of stomatal conductance
389 (Collatz et al., 1991) (see Table A3), the inverse of which we refer to as intrinsic water use
390 efficiency of photosynthesis (*iWUE*), following the definition of Beer et al., (2009). Even though
391 not all models use the BWBC model, we could estimate *m* and *iWUE* at the canopy scale for
392 those which simulate *GPP* in addition to *E*. We estimated *m* as the slope of the best fit line
393 between g_s and $GPP_{norm} = GPP^*(h/c_a)$ and took $iWUE = 1/m$, where c_a and *h* are ambient CO_2
394 mole fraction and relative humidity, respectively. Because the intercept of this relationship
395 across the majority of models and observations was near zero, we forced all fits through the
396 origin. While the flux tower observations were nearly linear, many models were slightly
397 nonlinear at high levels of GPP_{norm} and were also affected by outliers in g_s. We dealt with this
398 issue by fitting models with a 2^{nd} degree polynomial through the lower quantile of g_s (as
399 opposed to the mean of g_s which would have been affected by outliers) and estimated the slope

400 at an intermediate value of GPP_{norm} = 3.0 x 10^4 µmol m^{-2} s^{-1} where the fitted polynomial was
401 approximately linear. We estimated the uncertainty about observed *iWUE* as the inverse of the
402 upper and lower quartile fits of $m \sim GPP_{norm}$ and uncertainty in *GPP* as the pooled standard
403 deviation about the daily mean (across days and years). With estimates of *iWUE* and GPP_{norm},
404 we were able to address the degree to which some of the spread in the simulated magnitude of
405 *E* across models could be related to compensating errors in these variables which regulate
406 vegetation demand for water.
407
408 *2.6. Site and model representation in analyses*
409
410 Sites were represented in analyses as follows. For the first-order analysis of the
411 seasonality of *E* (Fig. 2) and its control by available energy (Fig. 3), we sought to show how the
412 sites behaved in accord to their site grouping along the north-south gradient of climate and
413 vegetation. In these figures, we present the observed and modeled data either averaged (Fig. 2)
414 or pooled (Fig. 3) within each site grouping. In analyses of supply (Fig. 4) and demand (Figs. 5 -
415 7), a site-specific approach was more appropriate because we were adjoining ancillary soil
416 moisture data or momentum and carbon fluxes to the water flux data. In these figures, we
417 selected one site to represent each of the three site groups. We selected K67 to represent the
418 equatorial forests since this site had the best data quality and coverage and because model-
419 model differences were most apparent at this site compared to K34 and K83. We selected the
420 seasonally flooded BAN site for the transitional forests in analyses of water supply because this
421 site behaved most differently when compared to the equatorial forest and Cerrado sites.
422 However, mechanisms of water supply at the BAN site should not be interpreted to be
423 characteristic of RJA or transitional forest sites in general. We used the RJA site to represent
424 transitional forest sites in the analyses of demand, since the assumption of negligible soil
425 evaporation at BAN is invalid. As the PDG site was the only Cerrado site, it is displayed in all
426 analyses to represent the Cerrado group.
427
428 Models were represented in analyses as follows. For the correlation analysis of

evapotranspiration with available energy (Fig. 3) and the analysis involving the mechanisms of supply (Fig. 4), we chose a subset of models which had added or changed different mechanisms hypothesized important for regulating the seasonality of *E*, and evaluated the effectiveness of these changes in improving subsequent model performance. These changes in structure fell into two main groups – 1) increases in soil and rooting depth beyond 3.5 meters, and 2) addition of a groundwater reservoir which was allowed to exchange water with unsaturated soil (as opposed to a standard free drainage bottom boundary condition). Within each of these two groups, we selected two models with versions prior to and following the associated structural change and the two models within each group were selected to illustrate the range of sensitivity to the structural change. This gave us a total of four unique "model families" and eight discrete model simulations on which we focused for the three sites. We selected the LPJ and SiB model families (LPJ-1.5m, LPJ-8m, SiB2, and SiB3 or SiBCASA) to illustrate the effect of implementing deep roots since the effect of adding deep roots was weakest in LPJ and strongest in SiB3 and SiBCASA. We selected the CLM and LEAF model families to illustrate the effect of adding interaction with groundwater since the strength of the effect for these models was different at different sites. Collectively, these models spanned the range of performance with respect to the observed seasonality of *E* (Fig. 2).

In the analysis of the mechanisms of vegetation demand, we first chose a subset of models at each of three different sites which simulated well the seasonality of observed *E* (SiB3, IBIS, JULES and ORCHIDEE at K67; SiBCASA, NOAH, LEAFHYDRO-WT and SiB3 at RJA; CLM3.5, ISAM, SiB3, SiBCASA and SSiB2 at PDG), in order to assess whether or not these models did so while also capturing the seasonality of canopy stomatal conductance (g_s). We then selected all models which simulated both carbon and water fluxes, except models which were run on a daily timestep (see Section 2.5), to assess how the combined g_s and intrinsic water use efficiency of photosynthesis (*iWUE*) mechanisms impacted the magnitude of modeled *E* (Fig. 7).

3. Results and Discussion

3.1. Seasonal cycles of E *across sites*

Figure 2 shows that equatorial forests exhibit a seasonal cycle of *E* peaking with net radiation during the dry season, transitional southern forests show either a flat seasonal cycle (due to less seasonality in available light) or a slight dry season depression (some degree of water limitation), and Cerrado demonstrates a strong dry season depression (both due to reductions in light and water). These results corroborate those of previous work which showed a general trend of increasing water limitation from north to south (Hasler and Avissar, 2007; Juarez et al., 2007; Borma et al., 2009; da Rocha et al., 2009; Fisher et al., 2009). While BAN and RJA differed slightly in their respective seasonalities of *E* (BAN has a more pronounced dry season depression compared to RJA), overall the individual site *E* seasonalities corresponded to the mean *E* seasonality of the grouped sites (see Appendix D of the Supplement for individual site seasonalities).

Models in general performed best at the end members of the precipitation gradient (Fig. 2a,c) but more poorly at transitional forest sites (Fig. 2b). In particular, models performed best at equatorial evergreen sites, with 13 and 15 out of 23 models capturing the observed magnitude and seasonality, respectively, of the mean *E* across these sites (Fig. 2a). Models comparatively performed most poorly at transitional forest sites (Fig. 2b) and to an intermediate degree at Cerrado (Fig. 2c).

3.2. Available energy as a driver of E

Cerrado demonstrated a clear contrast to equatorial and transitional forests in terms of how available energy controlled dry season *LE*, demonstrated by a significantly smaller slope of 0.51 +/- 0.03 (95% confidence interval) and coefficient of determination (R^2) value of 0.54 (Fig. 3 and Table 2). In other words, available energy during the dry season heats vegetation more in Cerrado compared to forests, and Cerrado vegetation is also less responsive to variations in available energy. The equatorial and transitional forests exhibited nearly the same partitioning

between *LE* and *H* during the dry season with slopes of 0.70 +/- 0.01 and 0.71 +/- 0.01, respectively (95% confidence intervals), but environmental factors other than available energy are apparently more involved in controlling variation in *LE* in transitional forests, evidenced by a lower R^2 value of 0.78 compared to 0.90 for equatorial forests (Table 2). In sum, the fraction of total variance in *LE* explained by available energy during the dry season moderately decreased with increasing strength of the dry season, presumably due to increasing degrees of dry season humidity or water deficits. Again, we emphasize relative differences in slopes and R^2 values across sites as opposed to absolute values. High dry season R^2 values at equatorial sites, however, did not preclude the role of vegetation demand (see Section 3.4).

For most models with shallow soil (LPJ-1.5m, SiB2, CLM3; all with soil depths < 3.5 m), available energy explained little of the total variance in *LE* in these models at all sites ($R^2 < 0.31$) (Fig. 2 and Table 2). The exception to this was LEAFHYDRO-NWT, which had much higher R^2 at equatorial sites but a low bias in its regression slope. When the shallow soil models were modified to have either deep soil or interaction with groundwater, they significantly improved dry season *LE* via increases in R^2 and slope, except for LPJ. Low infiltration capacity and high rates of surface runoff apparently limited the water available to deep soil and roots for sustaining *LE* during the dry season in this model (see Appendix D of the Supplement). For other models, fixing the supply side of the water limitation problem revealed significant positive biases in the partitioning of *LE* relative to *H* under non-water stressed conditions, evidenced by slopes exceeding those of the observations. At Cerrado, SiBCASA had a slope of 0.55 +/- 0.02 (not significantly greater than the observations) and at the equatorial forest sites CLM3.5 had a slope of 0.82 +/- 0.02, significantly greater than the observations (0.70 +/- 0.01) (Table 2; see also ED2, JULES, IBIS at Cerrado in Appendix C of the Supplement). Thus, it was not uncommon for models to "overfix" *E* when eliminating water limitation.

3.3. Supply-side mechanisms of E

Overall, models with soil depths less than or equal to 3.5 m and without groundwater

interaction were not able to simulate *E* without a dry season depression (Fig. 4b, d, g, i, l, n; see also Appendix D of the Supplement). Addition of an unconfined aquifer (CLM3.5, LEAFHYDRO-WT models) produced a similar effect on dry season water stress as did addition of deep soil and roots (LPJ-8m, SiB3, SiBCASA models). Increasing the soil depth or addition of an aquifer in most models decreased total runoff and increased the water storage capacity of soil (or soil-aquifer system, for models simulating one), providing a buffer for dry season deficits. In all instances where models erroneously predict a dry season depression in *E*, models overestimate wet season total runoff ($Q_s + Q_{sb}$) and underestimate wet season soil water storage (e.g., SiB2 & CLM3 models in Figs. 3-4). Therefore, we deem simulation of the seasonal patterns of soil moisture recharge and discharge critical to an accurate prediction of the seasonality of *E*. An exception to this was the LEAFHYDRO model, where addition of an aquifer was accompanied by an increase in drainage out of the soil column, but this was an artifact of a fixed water table depth in this model (seasonal water table variation in this model requires a representation of topography, and hence, was not possible with these 1D simulations) (Miguez-Macho and Fan, 2012).

At the equatorial evergreen forest site K67, SiB3 and CLM3.5 both had seasonal patterns of *E* that closely matched observations, but diverged in their simulated attribution of the soil water balance to seasonal patterns of soil moisture storage and runoff (Fig. 4c, e). SiB3 had large seasonal swings in stored soil moisture accompanied by a low rate of total runoff throughout the entire year, while CLM3.5 had lower seasonal variation in soil moisture, in addition to substantial dry season upward capillary flux ($Q_{g\uparrow}$) from groundwater (simulated water table depth was 3.6 – 4.8 m in this model).

A comparison to the water budget analysis derived from the observed seasonal cycles of *P*, *E*, and ΔS_s provides the necessary insight to discriminate among the dry season supply-side mechanisms used in the models. We infer a negligible role for upward capillary flux from a groundwater (does not exceed 18 mm month^{-1}) in regulating dry season *E* at the K67 equatorial forest site (Fig. 4a and Table 3). The observations indicated that soil moisture storage in the

545 unsaturated rooting domain to 11 m was able to endure a cumulative ~ 340 mm reduction to
546 sustain the dry season water deficit (Supplement Figure B4d). At this site, nearly all of the total
547 runoff (Q_s + Q_{sb}) occurs during the wet season months of Jan - May, with minimal drainage
548 during the dry season months Jun – Oct (i.e., nearly all of the reduction in soil moisture during
549 the dry season is due to root uptake). This stands in contrast with CLM3.5 (Fig. 4e) and other
550 models (Supplement Fig. D2) whose dry season *E* rates were sustained in part by capillary fluxes
551 from below the simulated rooting zone. Absence of shallow groundwater in the Tapajós region
552 is also corroborated by anecdotal evidence reported in the literature (reported at depths of ~
553 100 m in Nepstad et al., 2002; Belk et al., 2007), but it is important to note that water tables this
554 deep are not characteristic of Amazonia in general (Miguez-Macho and Fan, 2012). The
555 observations further bound the degree of seasonal variation in soil moisture predicted by deep-
556 root models (e.g., variation SiB3 is too large; Fig. 4c).
557
558 The transitional forest BAN differed dramatically in its seasonal hydrology from that at
559 K67; it has a shallow water table and floods during the wet season. Consequently, the two
560 model approaches (deep roots and groundwater) diverged in terms of the mechanism of dry
561 season water supply, despite similarities in their respective seasonalities of *E* (Fig. 4h, j).
562 LEAFHYDRO-WT with water table dynamics (Fig. 4j) simulates seasonal changes in water storage
563 and depletion entirely from groundwater instead of from the unsaturated rooting domain. SiB3
564 with deep roots (Fig. 4h), on the other hand, drew upon stored soil moisture from deep layers
565 (to 10m) to make up for dry season water deficits. While both models with these modifications
566 simulate the overall seasonality of *E* well, the observations indicated slight reductions in *E*
567 during the dry season in June through September, which were best captured by SiB3.
568
569 Surprisingly, the water budget analysis for the BAN site (Borma et al., 2009) revealed
570 that observed seasonal patterns of soil moisture storage and groundwater flux were not
571 consistent with either of the deep soil / deep roots or groundwater formulations (Fig. 4f,h,j).
572 While groundwater fluxes are significant (total annual influx of 211 mm $year^{-1}$), their timing
573 (almost all during the month of November) is not such that they contribute significantly to dry

574 season *E* (Table 3). Rather, stored soil moisture to 2m depth is more than sufficient to supply
575 the entire dry season *E* water deficit, evidenced by reductions in soil moisture which exceed *E*
576 losses, resulting in significant total runoff ($Q_s + Q_{sb}$) occurring throughout the dry season (Fig.
577 4f). A large influx of groundwater into the system is inferred during the month of November
578 because soil water increases by nearly double the incoming precipitation, even when the soil
579 moisture measurements are not extrapolated beyond the measurement domain (Table 3). The
580 abrupt influx of groundwater ($Q_{g\uparrow}$) into this system occurs not because of soil type or depth, but
581 because of this site's proximity to a floodplain (Borma et al., 2009), and no further net influx of
582 groundwater after November is recorded because the soil quickly becomes and remains
583 saturated throughout the flooding period. This highlights the importance of modeling
584 groundwater fluctuations as a 2-dimensional topographically-driven process, in which
585 orientation in relation to drainage basins makes a big difference (Fan and Miguez-Macho, 2010).
586 On the other hand, the role of persistent deep roots regulating *E* at this site is likely also be
587 limited, given the presumed anoxic soil conditions which persist during the flooding period.
588
589 At the Cerrado site PDG, we inferred a small (16 mm month^{-1}) upward groundwater flux
590 during the dry season months of June and July (Fig. 4k). However, this is probably an artifact
591 and likely represents root uptake below 2.5 m. Soil moisture measurements extended to a
592 depth of 2.5 m only at this site (Table 1) and we were unable to extrapolate variations in soil
593 moisture beyond this depth (see Appendix B of the Supplement). We argue that the 16 mm
594 month^{-1} water flux during these months actually represents deep root uptake (beyond 2.5 m)
595 because a large dry season reduction in soil moisture content still occurs at 2.5 m (Supplement
596 Fig. B1) and there is no reason to believe such seasonal variability would not continue at depths
597 beyond 2.5 m, but this needs to be tested with deeper soil moisture measurements.
598 Regardless, this site still demonstrated a significant degree of water stress, evidenced by a
599 substantial depression in *E* during the dry season, in phase with reductions in available energy
600 (R_n), but with a substantial fraction of variation in *E* left unexplained and a smaller evaporative
601 fraction (lower R^2 and slope in Fig. 3a). The SiB2 and LEAFHYDRO-NWT models underestimated
602 dry season *E* in the absence of any deep rooting or groundwater mechanisms (Fig. 4l, n). Unlike

what was observed at equatorial and transitional sites, however, model results at this site showed that inclusion of deep soil / roots or groundwater mechanisms did not produce similar dry season patterns in *E*; only the deep roots mechanism was able to significantly increase dry season *E* (Fig. 4m). The model results thus suggest that deep roots indeed play an important role in maintaining dry season *E*. Nonetheless, the simulated magnitude of the effect that deep roots has in supplying dry season *E* is still often overestimated (e.g., SiBCASA Fig. 4m and JULES, IBIS Supplement Fig. D6), revealing model errors with respect to vegetation demand, which we discuss in the next section.

Potential limitations in this analysis are predominantly associated with the estimation of total soil moisture from the observational data. In some cases, the period of available soil moisture observations did not exactly coincide with the flux tower observations (Table 1). However, our use of the seasonal cycle helped to mitigate this problem. Errors associated with this likely are to be concentrated at wet/dry season boundaries; but we focused our interpretation based on coarse wet versus dry season patterns, limiting the possibility of making erroneous conclusions. Furthermore, at the one site (BAN) where we infer important groundwater fluxes at the seasonal boundaries, the soil moisture observations corresponded to 2 out of the 3 years of available flux tower data (Table 1).

The second source of uncertainty associated with the use of the soil moisture data are the estimates of upward capillary flux. The method of estimating the observed water budget also makes an estimate of the contribution of an upward capillary water flux ($Q_{g\uparrow}$) to dry season evapotranspiration, which in most months is a small fraction of total *E*. Such an upward capillary flux is inferred when the dry season water deficit ($P - E$) is not matched by a corresponding reduction in root zone soil moisture. To be clear, such an estimate likely underestimates the total upward capillary flux, since it represents only that portion of the capillary flux used by evapotranspiration. Absence of inferred capillary flux also does not necessarily rule out the role of an aquifer, either. While there may be no inferred upward capillary flux (i.e., total water potential does not increase with depth), saturated soil below an

632 unsaturated root zone should reduce the downward rate of drainage relative to that expected
633 from free drainage (i.e., matric water potential increases with depth, thus reducing the rate at
634 which total water potential decreases with depth).
635
636 In summary, models which simulated an aquifer tended to do so at the expense of
637 simulating seasonal swings in root zone soil moisture, often at odds with observations. On the
638 other hand, models using a free drainage bottom boundary condition were able to mitigate the
639 effects of excessive dry season drainage on water stress by employing a deep soil column with
640 deep roots to access the larger total volume of water available for uptake, without fixing the
641 drainage problem *per se*. Thus, while accurately simulating the annual cycle of *E*, the net effect
642 in these models was to overestimate seasonal variability in soil moisture by overestimating dry
643 season subsurface drainage. Given the role of accurately simulating total runoff and soil
644 moisture for the accurate prediction of seasonal *E* patterns, the deep soil / groundwater
645 tradeoff highlights the fact that the choice of a bottom boundary condition in LSMs is not trivial
646 (Gulden et al., 2007). Whatever the correct bottom boundary condition may be, the associated
647 deep drainage appears to be somewhere in between that predicted by a free drainage and a
648 saturated bottom boundary condition (Zeng & Decker 2010).
649
650 We conclude that the mechanisms of upward capillary flux and deep root uptake are
651 complementary and can both sustain *E* during the dry season, but their relative importance is
652 site-dependent. For example, deep soils on plateaus, such as those in the Tapajós region and
653 throughout much of eastern Amazônia have water table depths at 10-40 m (Fan and Miguez-
654 Macho, 2010), also have been documented to have deep roots (Nepstad et al., 1994), though
655 the ubiquity of a deep rooting habit across species remains unknown. In contrast, at sites like
656 RJA (Supplement Fig. D4) and BAN which either have shallower soils or are proximal to drainage
657 basins, the functional role of deep roots is dubious, and combined moisture storage and
658 subsurface lateral flow is more important in regulating dry season water deficits. The CLM3.5
659 and LEAFHYDRO-WT models were run as single-point runs, and, as noted above, LEAFHYDRO is
660 designed to capture the two-dimensional nature of groundwater flux while CLM3.5

parameterizes the exchange of soil water with groundwater using only one dimension, in the vertical. Vertical exchange in CLM3.5 is dependent on precipitation climatology alone, while in LEAFHYDRO, lateral convergence due to horizontal gradients in both climatology and topography are considered. For BAN, however, the role of groundwater may be to contribute to storage to the unsaturated zone at the onset of the wet season (as opposed to dry season capillary flux) which may then be drawn upon the subsequent dry season. More root zone soil moisture measurements combined with estimates of *E* and *P*, as well as improved knowledge of soil hydraulic properties at other sites across Amazonia are needed to address how prominent dry season capillary fluxes are in contributing to dry season *E*.

3.4. Demand-side mechanisms of E_t

In Fig. 5a, b, and c, we have shown at each of three sites the models which simulated well the seasonality and magnitude of transpiration (E_t). The trend in seasonality of E_t for the observations goes from a dry season peak in an equatorial forest (K67) to near-flat seasonality in a transitional forest (RJA), to a dry season depression in Cerrado (PDG), similar to that of evapotranspiration (*E*) (Fig. 2). In contrast, the seasonality of canopy stomatal conductance (g_s) exhibits varying degrees of a dry season depression at all sites (Fig. 5d, e, f), implying that regulation of water demand by vegetation persists even in the moist equatorial forests (Costa et al., 2010). While the(Meinzer, 1993) models captured the overall shifts across sites in the magnitude of vegetation demand (i.e., g_s) reasonably well (Fig. 6d, e, f), many of these otherwise well-performing models did not capture the appropriate seasonality of g_s (e.g., SiB3, JULES, IBIS at K67; SiB3, SiBCASA, LEAFHYDRO-WT at RJA). Additionally, some models demonstrated biases in the magnitude of g_s at individual sites (e.g., IBIS at K67, LEAFHYDRO-WT at RJA). Below we explore some potential reasons for these model errors.

While higher dry season vapor pressure deficit (*D*) regulates the seasonality of g_s to a certain degree at the leaf level, leaf phenology regulates the quantity and physiological efficiency of leaves at the canopy level, and thus also may regulate the seasonality of whole

ecosystem vegetation demand for water. Differences in the timing of the minimum observed g_s at K67 compared to that of other sites suggest that canopy dynamics indeed play a role. While the minimum observed g_s at RJA and PDG occurs when the dry season is most intense (Fig. 5 e, f; i.e., when precipitation and *D* reach their respective minima and maxima), the minimum g_s at K67 occurs at the beginning of the dry season, and remains constant or slightly recovers throughout the remainder of the dry season (Fig. 5 d) as water deficits (both soil and atmospheric *D*) continue to rise. Comparison of the seasonality of g_s to that of LAI at a nearby (~ 3 km) site (Brando et al., 2010) revealed that the timing of the minimum in g_s at K67 lags 1 month that of LAI (Fig. 5g), and high rates of litterfall are also coincident with increasing dry season LAI at the K67 site, implying a period of significant leaf flush. We found that a significant positive relationship ($p < 0.05$) exists between g_s and LAI when g_s is lagged by one month (inset Fig. 5g), roughly the amount of time required for new leaf expansion. This corroborates recent work (Restrepo-Coupe et al., 2013) which demonstrates the importance of canopy leaf flush driving the seasonality of photosynthesis across the Amazon basin. In contrast to these observations, many models which captured the seasonality of *E* consistently underestimated seasonal variability in g_s. Collectively, this suggests that the discrepancy between observed and modeled seasonality of vegetation water demand at equatorial and transitional forest sites K67 and RJA is due in part to such biological rhythms of leaf phenology, a process poorly represented in vegetation models.

Other models which simulated well both the seasonality and magnitude of E_t at times exhibited a systematic low bias in the magnitude of g_s. An exploration of the canopy temperatures (T_v) of some of these models (IBIS at K67, LEAFHYDRO at RJA) revealed a corresponding warm bias (see arrows in Fig. 6). These models are able to capture the magnitude of *E* and E_t at these sites presumably because this warm bias contributes to a larger vapor pressure deficit in these models which, given the same atmospheric conditions, drives a larger vapor flux at low g_s. The counteracting effect of T_v bias, however, was not enough to offset more extreme biases in g_s in other models, resulting in corresponding errors in simulated E_t. For example, warm-biased models ED2 and CN-CLASS (Fig. 6a, b) consistently

719 underestimated E_t. Finally, two models which run at a daily timestep, LPJ and Biome-BGC, use
720 mean air temperatures to estimate leaf temperature, and as a consequence of disregarding
721 diurnal variability in temperature and radiative heating at the leaf surface, they consistently
722 underestimated daytime canopy temperatures at all sites (Fig. 6a, b, c). Simple formulations of
723 canopy temperature using information on diurnal air temperature ranges could be readily
724 employed to ameliorate this bias. In sum, these examples emphasize how biases in canopy
725 temperature can have important consequences for vegetation water demand. Furthermore,
726 models must accurately simulate vapor fluxes at the right canopy temperature because of the
727 temperature dependency of photosynthesis (Rubisco activity, light capture) and leaf respiration.
728
729 In addition to canopy stomatal conductance, the intrinsic water use efficiency of
730 photosynthesis (*iWUE*), or photosynthesis per unit stomatal conductance, is also an important
731 control on vegetation water demand. Higher (lower) *iWUE* implies vegetation is
732 photosynthesizing at a lower (higher) internal to ambient CO_2 ratio (Lloyd et al., 2002; Beer et
733 al., 2009), and its variation across sites in Amazonia and Cerrado may reflect site differences in
734 soil fertility, vegetation composition, or both. It is an important diagnostic for modeled *E* in
735 addition to g_s because it governs how the light response of photosynthesis is translated into
736 evaporative losses. To demonstrate the interaction between *GPP* and *iWUE* on simulated
737 magnitudes of *E*, in Fig. 7 we have arrayed models in a '*GPP – iWUE* space' for select sites across
738 the climate and vegetation composition gradient (K67, RJA, and PDG), with simulated
739 magnitudes of transpiration (E_t) represented by color: models in black text simulated a mean E_t
740 within the observed mean E_t +/- 0.5 mm d^{-1}, and models in red and blue text fell below and
741 above this range, respectively.
742
743 Mean site *GPP* decreased with E_t along the climate and vegetation composition gradient
744 from equatorial forests to Cerrado, but there was no systematic trend in *iWUE* across the
745 gradient (Fig. 7). The lack of a difference in *iWUE* between forest and Cerrado at an annual
746 average scale does not preclude the existence of differences in the seasonality of *iWUE* across
747 sites, which we did not analyze. Still, this analysis demonstrates that site-site differences in the

magnitude of *E* are not due to differences in *iWUE*; rather, the drivers of the magnitude of *E* appear to be common to those controlling the magnitude of *GPP*. The PDG Cerrado site has a GPP (mean +/- 95% confidence interval) of 8.2 +/- 1.4 μmol CO_2 m^{-2} s^{-1} which is less than half that of RJA (7.7 +/- 1.8 μmol CO_2 m^{-2} s^{-1}) or K67 (3.2 +/- 1.7 μmol CO_2 m^{-2} s^{-1}). It is possible that the low soil fertility of Cerrado (Furley and Ratter, 1988) combined with its substantially different species composition (Lloyd et al., 2009) places additional constraints on photosynthesis beyond those of climate alone. These additional constraints on photosynthesis are then translated into a reduced water vapor flux because *iWUE* did not change significantly between Cerrado and forest.

Consequently, models which failed to capture constraints on photosynthesis also had positive biases in their simulated transpiration (E_t). For instance, the CLM3.5 and ORCHIDEE models overestimated GPP at RJA while IBIS and JULES overestimated GPP at PDG, causing these models to overestimate water flux at these sites (Fig. 7b, c). IBIS and JULES were previously noted to "overfix" modeled *E* in Cerrado and it is clear that they do so by overestimating the light response of photosynthesis, i.e., *GPP*, as opposed to underestimating *iWUE*. Many otherwise well-performing models in terms of their simulated E_t were not able to capture variations in *GPP* and *iWUE* in concert across sites. This problem was especially apparent in Cerrado, where models such as SSiB2, ORCHIDEE, SiBCASA, CLM3.5 and ED2 overestimated *GPP* while also overestimating *iWUE*, which allowed them to simulate the appropriate magnitude of E_t, but with the incorrect mechanisms (Fig. 7c). Overall model spread in *GPP* was greatest in the transitional forest of RJA (Fig. 7b), while model spread in *iWUE* was also large, both of which combine to explain the large model spread in simulated *E* in transitional forests (Fig. 2b). In contrast, most of the model spread in simulated *E* in equatorial forests (Fig. 2a) is due to variation in simulated *iWUE*, not *GPP*, as evidenced by the K67 site (Fig. 7a).

One of the reasons for model bias in *iWUE* can simply be attributed to parameter values in their associated stomatal closure equation (equations and parameters given in Table A3). For

777 instance, ED2, IBIS and CNCLASS tended to overestimate *iWUE* because of lower values of *m*,
778 equal to 8, 8, and 6, respectively. It should be noted that one model (ISAM) was able to capture
779 most of the variation in the magnitude of E_t across sites with the appropriate mechanistic
780 responses of *iWUE* and *GPP* (Figs. 7b, c). This model incorporates nutrient (nitrogen) cycles into
781 whole-system biogeochemical processes, including photosynthesis (Thornton, et al., 2007; Jain
782 et al., 2009; Bonan et al., 2011) and associated stomatal responses. The CLM4-CN model, also a
783 model incorporating nutrient cycling, also captures the variation in *E*, *iWUE*, and *GPP* across
784 sites, except for a small positive bias in *GPP* at K34.(Quesada et al., 2012)
785
786 These results highlight the challenge facing models not to improve simulations of
787 tropical forests at the expense of Cerrado. That Cerrado would exhibit dynamics not easily
788 represented by models which were improved with tropical forests in mind should not be
789 surprising; Cerrado is quite far from being analogous to seasonally dry forest both in terms of
790 phylogenetic distance (Pennington et al., 2000; Pennington et al., 2009) and species functional
791 traits (Hoffmann et al., 2012). Models which captured some of the biome differences in *E* as
792 well as *GPP* and *iWUE* were models which account for nutrient limitations on forest and
793 savanna ecophysiology, but we did not do the necessary analyses to confirm this as fact.
794 Nevertheless, this supports recent evidence that basin-wide variation in nutrients play an
795 important role in governing patterns in productivity (Quesada et al., 2012) and by extension,
796 evapotranspiration. Regardless, model improvements in Cerrado and its boundary with forest
797 will require modeling the synergistic effects of soil fertility and disturbance via fire, since these
798 mechanisms are the primary factors controlling the relative productivity and abundance of trees
799 and grasses at this ecotone (Furley and Ratter, 1988; Ratter, 1992).
800
801 *3.5. Model benchmarking*
802
803 We have shown that models can simulate the correct magnitude and seasonality of *E*
804 from equatorial Amazonia to Cerrado using multiple supply and demand side mechanisms, and
805 the observations have provided important constraints these mechanisms. A single

806 comprehensive metric of performance for each model with respect to simulated magnitudes
807 and seasonalities of *E* that integrates both supply and demand regulatory mechanisms is
808 beyond the scope of this paper. However, based on our analysis of demand-side mechanisms
809 with respect to the magnitude of E_t, we present what a model benchmark might look like in
810 Table 4. For equatorial (K34, K67, K83), transitional (RJA only), and Cerrado (PDG) sites, models
811 and observations are ordered by increasing magnitude of transpiration (E_t) (not an annual
812 mean). We then summarize whether or not models simulated with high or low bias, or within
813 observational error, the four variables regulating vegetation water demand (g_s, T_v, *GPP*, *iWUE*)
814 in columns 1-4, in addition to E_t (column 7). A model which simulates a magnitude of E_t within
815 the observational error while also simulating the four demand variables within observational
816 error, we deem does so "for the right reasons" (column 8), at least with respect to demand-side
817 mechanisms regulating vegetation water demand.
818
819 Six, six, and 11 models "get the right answer" at the equatorial forest sites, the RJA
820 transitional forest site, and the PDG Cerrado site, respectively: that is, they simulate the
821 magnitude of E_t to within +/- 0.5 mm day^{-1} of the observations (Table 4). At none of these sites,
822 however, did a majority of these models do so for the right reasons. PDG was the site with the
823 greatest number of models (five) doing so for the right reasons, but only two of these models
824 were models which also simulated carbon fluxes. In sum, the model benchmark has identified
825 model deficiencies which would not have otherwise been apparent based on a simple model-
826 data comparison of evapotranspiration flux.
827
828 **4.** Conclusions
829
830 This study was undertaken to accomplish two main objectives: First, to establish how
831 mechanisms of water supply and vegetation water demand control evapotranspiration (*E*) along
832 a climate and vegetation composition gradient from equatorial Amazonia to Cerrado; and
833 second, to evaluate these mechanisms in a suite of ecosystem models. Encouragingly, most
834 models are now able to simulate with relative accuracy the magnitude and seasonality of *E* at

835 equatorial sites and Cerrado, but transitional forests continue to pose challenges for models.
836 However, we identified some deficiencies in models which would not otherwise be apparent
837 based on a simple comparison of simulated and observed magnitude and seasonal cycle of *E*.
838
839 We showed that the mechanisms of upward capillary flux and deep root uptake are
840 complementary mechanisms of water supply and can both sustain *E* during the dry season, but
841 their relative importance is site-dependent. Some models prescribed deep roots at all sites
842 (e.g., LPJ-8m) or manipulated rooting depth via optimization/sensitivity analysis (e.g., BIOME-
843 BGC, ORCHIDEE, SiB3, IBIS), while others (e.g., CLM, ISAM, NOAH-MP) relied on groundwater
844 recharge based solely on precipitation climatology and soil texture, to make up for dry season
845 water deficits. In contrast, the observations indicated that the relative importance of these two
846 mechanisms did not vary as a simple function of climate or location along the climate and
847 vegetation composition gradient. Consequently, models often simulated well the seasonality of
848 *E*, but with the incorrect mechanism of water supply. While the real principles which govern the
849 relative magnitude of deep root activity and capillary fluxes remain to be elucidated, contrasting
850 the LEAFHYDRO-WT point simulations analyzed here with results from a previous study
851 (Miguez-Macho and Fan, 2012) suggests that both the magnitude *and* seasonal timing of
852 capillary fluxes is governed just as much by local topography and proximity to drainage basins as
853 by climatology and soil texture. Capturing these effects in models, therefore, will require not
854 only simulation of lateral subsurface water flow (a two-dimensional process), but spatial
855 resolutions much higher than the typical GCM simulation (1^o x 1^o). Most importantly, however,
856 the analysis of water supply highlights unanswered questions regarding deep root activity, both
857 from an ecological point of view as to which trade-offs govern deep roots (as a plant trait)
858 within and across tropical forest communities, and from a mechanistic view as to the
859 significance of these deep roots in water and nutrient uptake.
860
861 We also showed that, while most equatorial and transitional forests demonstrated a
862 seasonal cycle of transpiration (E_t) which closely followed that of net radiation, vegetation water
863 demand via canopy stomatal conductance was still a moderate to significant control. Some

models, however, which simulated well the seasonal cycle of E_t and its control by net radiation did so with near-constant canopy stomatal conductance throughout most of the year. We presented evidence at an equatorial site(Restrepo-Coupe et al., in press) which suggests that the quantity and age distribution of leaves in the canopy plays just as significant a role in the seasonality of canopy stomatal conductance as does leaf-level stomatal control, implying that some of the data-model discrepancy is due to leaf phenology, a process poorly represented in vegetation models. Model biases in the magnitude of canopy stomatal conductance, in turn, could be related to light response (*GPP*) or the intrinsic water use efficiency of photosynthesis (*iWUE*), in addition to its effect on canopy temperatures. We found that most of the variation in modeled rates of *E* at an equatorial site was explained by *iWUE*, but at Cerrado, many models were characterized by a "cryptic bias", i.e., biases in both *iWUE* and *GPP* partially cancelled each other out, leading to modeled magnitudes of *E* indistinguishable from the observations. While modeled *E* bias at the equatorial site can be remedied by a simple optimization scheme tuning the magnitude of the Ball-Berry parameter *m*, model issues at Cerrado would require better parameterization of both Vcmax (light response) and *m*.

Most importantly, these analyses highlight how model improvements need to focus on biological controls on *E* in addition to physical mechanisms, especially given the predominance of transpiration fluxes in total evapotranspiration (Jasechko et al., 2013). This will require continued and expanded efforts to monitor root and canopy demographic processes in relation to variability in available water, nutrients and light. These efforts will realize maximum benefit when conducted at sites with existing ecosystem-level eddy covariance measurement infrastructure, allowing these sub-scale processes to inform controls on ecosystem-level processes. Integrating these biological responses and feedbacks to the processes of water cycling, therefore, will improve our understanding of vegetation-climate feedbacks in the tropics.

Acknowledgments

Author contributions. First author BOC and senior author SRS designed the analyses. BOC conducted the analyses. Second author NRC provided BrasilFlux database support. BOC

and SRS wrote the paper with contributions from NRC, PC, JBF, DG, LG, GM-M, BP, KSa, KSc, HV, Z-LY, BK, MHC, and XZ. Model output and contributions to model classification were provided by MAA, ITB, BPC, JBF, DG, XG, LG, BvdH, KI, HI, AJ, NL, GM-M, BP, DRR, KSa, AS, KSc, MS, HV and Z-LY. Key datasets and insights into their appropriate analysis were contributed by ACA, BK, AOM, HRdR and CvR. LBA-DMIP project was coordinated by MNM, JB, MHC, LGGdG, XZ and SRS.

This research was funded by the National Aeronautics and Space Administration (NASA) (LBA investigation CD-32 and the LBA-DMIP project, award #NNX09AL52G), the National Science Foundation (Amazon-PIRE, NSF award #OISE-0730305), and the Gordon and Betty Moore Foundation's Andes-Amazon Initiative. HRdR acknowledges FAPESP (08-581203) for aiding field data collection. Soil moisture data for the RJA field site were collected under the ABRACOS project and made available by the UK Institute of Hydrology and the Instituto Nacional de Pesquisas Espaciais (Brazil). ABRACOS was a collaboration between the Agencia Brasileira de Cooperação and the UK Overseas Development Administration. BOC acknowledges support from a Graduate Research Environmental Fellowship (GREF) - U.S. DOE Global Change Education Program, as well as an NSF Amazon-PIRE fellowship. JBF contributed to this paper from the Jet Propulsion Laboratory, California Institute of Technology, under a contract with the National Aeronautics and Space Administration. We thank Reto Stoeckli for initial generation of gap-filled meteorological driver data, and Enrique Rosero for discussions helping to frame some analyses for this paper. We are indebted to both LBA and ABRACOS projects, and their field technicians, without whose efforts to establish and preserve the quality of datasets used here, this paper would not have been possible. We are grateful to two anonymous reviewers whose comments greatly improved the clarity of this paper.

References

Avissar, R. and Werth, D., 2004. Comments on "The regional evapotranspiration of the Amazon'' - Reply. Journal of Hydrometeorology, 5(6): 1281-1281.

Baker, I.T. et al., 2008. Seasonal drought stress in the Amazon: Reconciling models and observations. Journal of Geophysical Research, 113.

Baldocchi, D., Luxmoore, R.J. and Hatfield, J.L., 1991. Discerning the forest from the trees: an essay on scaling canopy stomatal conductance. Agricultural and Forest Meteorology, 54: 197-226.

Ball J.T., Woodrow I.E. & Berry J.A. (1987) A model predicting stomatal conductance and its contribution to the control of photosynthesis under different environmental conditions. In: *Progress in Photosynthesis Research* (ed I. Biggins), pp. 221-224. Martinus Nijhoff, Netherlands.

Balsamo, G. et al., 2009. A Revised Hydrology for the ECMWF Model: Verification from Field Site to Terrestrial Water Storage and Impact in the Integrated Forecast System. Journal of Hydrometeorology, 10(3): 623-643.

Beer, C. et al., 2009. Temporal and among-site variability of inherent water use efficiency at the ecosystem level. Global Biogeochemical Cycles, 23(2).

Best, M.J. et al., 2011. The Joint UK Land Environment Simulator (JULES), model description - Part 1: Energy and water fluxes. Geoscientific Model Development, 4(3): 677-699.

Betts, R.A. et al., 2004. The role of ecosystem-atmosphere interactions in simulated Amazonian

precipitation decrease and forest dieback under global climate warming. Theoretical and Applied Climatology, 78(1-3): 157-175.
Bonan, G., 1998. The land surface climatology of the NCAR Land Surface Model coupled to the NCAR Community Climate Model. Journal of Climate, 11: 1307-1326.
Borma, L.S. et al., 2009. Atmosphere and hydrological controls of the evapotranspiration over a floodplain forest in the Bananal Island region, Amazonia. Journal of Geophysical Research-Biogeosciences, 114: G01003.
Brando, P.M. et al., 2010. Seasonal and interannual variability of climate and vegetation indices across the Amazon. Proceedings of the National Academy of Sciences, 107(33): 14685-14690.
Bruno, R.D., da Rocha, H.R., de Freitas, H.C., Goulden, M.L. and Miller, S.D., 2006. Soil moisture dynamics in an eastern Amazonian tropical forest. Hydrological Processes, 20(12): 2477-2489.
Buckley, T.N., 2005. The control of stomata by water balance. New Phytologist, 168(2): 275-292.
Clapp, R.B. and Hornberger, G.M., 1978. Empirical equations for some soil hydraulic properties. Water Resources Research, 14(4): 601-604.
Clark, D.B. et al., 2011. The Joint UK Land Environment Simulator (JULES), model description - Part 2: Carbon fluxes and vegetation dynamics. Geoscientific Model Development, 4(3): 701-722.
Collatz, G.J., Ball, J.T., Grivet, C. and Berry, J.A., 1991. Physiological and environmental regulation of stomatal conductance, phtosynthesis and transpiration: a model that includes a laminar boundary layer. Agricultural and Forest Meteorology, 54: 107-136.
Costa, M.H. et al., 2010. Atmospheric versus vegetation controls of Amazonian tropical rain forest evapotranspiration: Are the wet and seasonally dry rain forests any different? Journal of Geophysical Research-Biogeosciences, 115.
Costa, M.H., Souza, J.D.C. and Ribeiro, A., 2004. Comments on "The regional evapotranspiration of the Amazon''. Journal of Hydrometeorology, 5(6): 1279-1280.
Cox, P.M., Huntingford, C. and Harding, R.J., 1998. A canopy conductance and photosynthesis model for use in a GCM land surface scheme. Journal of Hydrology, 212-213: 79-94.
Cox, P.M., Betts, R.A., Jones, C.D., Spall, S.A. and Totterdell, I.J., 2000. Acceleration of global warming due to carbon-cycle feedbacks in a coupled climate model. Nature, 408: 184-187.
da Rocha, H.R. et al., 2002. Measurements of CO exchange over a woodland savanna (Cerrado sensu stricto) in southeast Brasil. Biota Neotropica, 2(1): BN01702012002.
da Rocha, H.R. et al., 2009. Patterns of water and heat flux across a biome gradient from tropical forest to savanna in Brazil. Journal of Geophysical Research-Biogeosciences, 114.
de Gonçalves, L.G.G. et al., 2013. Overview of the Large-Scale Biosphere–Atmosphere Experiment in Amazonia Data Model Intercomparison Project (LBA-DMIP). Agricultural and Forest Meteorology, 182-183: 111-127.
de Rosnay, P. and Polcher, J., 1998. Modelling root water uptake in a complex land surface scheme coupled to a GCM. Hydrology and Earth System Sciences, 2(2-3): 239-255.
Dickinson, R.E. et al., 2006. The Community Land Model and its climate statistics as a component of the Community Climate System Model. Journal of Climate, 19(11): 2302-2324.

Ducoudre, N.I., Laval, K. and Perrier, A., 1993. Sechiba, a New Set of Parameterizations of the Hydrologic Exchanges at the Land Atmosphere Interface within the Lmd Atmospheric General-Circulation Model. Journal of Climate, 6(2): 248-273.

Eltahir, E.A.B. and Bras, R.L., 1994. PRECIPITATION RECYCLING IN THE AMAZON BASIN. Quarterly Journal of the Royal Meteorological Society, 120(518): 861-880.

Fan, Y. and Miguez-Macho, G., 2010. Potential groundwater contribution to Amazon evapotranspiration. Hydrology and Earth System Sciences, 14(10): 2039-2056.

Fisher, J.B. et al., 2009. The land-atmosphere water flux in the tropics. Global Change Biology, 15(11): 2694-2714.

Foley, J.A. et al., 1996. An integrated biosphere model of land surface processes, terrestrial carbon balance, and vegetation dynamics. Global Biogeochemical Cycles, 10(4): 603-628.

Furley, P.A. and Ratter, J.A., 1988. Soil resources and plant communities of the central Brazilian cerrado and their development. Journal of Biogeography, 15(1): 97-108.

Galbraith, D. et al., 2010. Multiple mechanisms of Amazonian forest biomass losses in three dynamic global vegetation models under climate change. New Phytologist, 187(3): 647-665.

Gerten, D., Schaphoff, S., Haberlandt, U., Lucht, W. and Sitch, S., 2004. Terrestrial vegetation and water balance—hydrological evaluation of a dynamic global vegetation model. Journal of Hydrology, 286(1-4): 249-270.

Grant, R.F. et al., 2009. Modeling the carbon balance of Amazonian rain forests: resolving ecological controls on net ecosystem productivity. Ecological Monographs, 79(3): 445-463.

Gulden, L.E. et al., 2007. Improving land-surface model hydrology: Is an explicit aquifer model better than a deeper soil profile? Geophysical Research Letters, 34(9).

Harper, A.B. et al., 2010. Role of deep soil moisture in modulating climate in the Amazon rainforest. Geophysical Research Letters, 37.

Hasler, N. and Avissar, R., 2007. What controls evapotranspiration in the amazon basin? Journal of Hydrometeorology, 8(3): 380-395.

Haxeltine, A. and Prentice, I.C., 1996. BIOME3: An equilibrium terrestrial biosphere model based on ecophysiological constraints, resource availability, and competition among plant functional types. Global Biogeochemical Cycles, 10(4): 693-709.

Hodnett, M.G., Pimentel da Silva, L., da Rocha, H.R. and Cruz Senna, R., 1995. Seasonal soil water storage changes beneath central Amazonian rainforest and pasture. Journal of Hydrology, 170: 233-254.

Hoffmann, W.A. et al., 2012. Ecological thresholds at the savanna-forest boundary: how plant traits, resources and fire govern the distribution of tropical biomes. Ecology Letters, 15(7): 759-768.

Huntingford, C. et al., 2008. Towards quantifying uncertainty in predictions of Amazon 'dieback'. Philosophical Transactions of the Royal Society B-Biological Sciences, 363(1498): 1857-1864.

Ichii, K. et al., 2007. Constraining rooting depths in tropical rainforests using satellite data and ecosystem modeling for accurate simulation of gross primary production seasonality. Global Change Biology, 13(1): 67-77.

Jacobs, C.M.J., 1994. Direct impact of atmospheric CO2 enrichment on regional transpiration.,

Wageningen Agricultural University.
Jarvis, P.G., 1976. The interpretation of the variations in leaf water potential and stomatal conductance found in canopies in the field. Philosophical Transactions of the Royal Society B: Biological Sciences, 273(927): 593-610.
Jasechko, S. et al., 2013. Terrestrial water fluxes dominated by transpiration. Nature, 496(7445): 347-350.
Juarez, R.I.N., Hodnett, M.G., Fu, R., Goulden, M.L. and von Randow, C., 2007. Control of dry season evapotranspiration over the Amazonian forest as inferred from observations at a southern Amazon forest site. Journal of Climate, 20(12): 2827-2839.
Krinner, G. et al., 2005. A dynamic global vegetation model for studies of the coupled atmosphere-biosphere system. Global Biogeochemical Cycles, 19(1): doi:10.1029/2003GB002199.
Lee, J.E., Oliveira, R.S., Dawson, T.E. and Fung, I., 2005. Root functioning modifies seasonal climate. Proceedings of the National Academy of Sciences of the United States of America, 102(49): 17576-17581.
Leuning, R., Kelliher, F.M., Depury, D.G.G. and Schulze, E.D., 1995. Leaf Nitrogen, Photosynthesis, Conductance and Transpiration - Scaling from Leaves to Canopies. Plant Cell and Environment, 18(10): 1183-1200.
Lloyd, J. et al., 2009. Ecophysiology of Forest and Savanna Vegetation. In: M. Keller, M. Bustamente, J. Gash and P. Silva Dias (Editors), Amazonia and Global Change, Geophysical Monograph Series. AGU, Washington, D. C.
Lloyd, J. et al., 2002. Seasonal and annual variations in the photosynthetic productivity and carbon balance of a central Siberian pine forest. Tellus, 54B: 590-610.
Medvigy, D., Wofsy, S.C., Munger, J.W., Hollinger, D.Y. and Moorcroft, P.R., 2009. Mechanistic scaling of ecosystem function and dynamics in space and time: Ecosystem Demography model version 2. Journal of Geophysical Research, 114(G1).
Miguez-Macho, G. and Fan, Y., 2012. The role of groundwater in the Amazon water cycle: 2. Influence on seasonal soil moisture and evapotranspiration. Journal of Geophysical Research-Atmospheres, 117.
Monteith, J.L., 1995. Accomodation between transpiring vegetation and the convective boundary layer. Journal of Hydrology, 166: 251-263.
Nepstad, D.C. et al., 1994. The role of deep roots in the hydrological and carbon cycles of Amazonian forests and pastures. Nature, 372(6507): 666-669.
Nepstad, D.C. et al., 2002. The effects of partial throughfall exclusion on canopy processes, aboveground production, and biogeochemistry of an Amazon forest. Journal of Geophysical Research, 107(D20).
Niu, G.-Y. et al., 2011. The community Noah land surface model with multiparameterization options (Noah-MP): 1. Model description and evaluation with local-scale measurements. Journal of Geophysical Research, 116(D12).
Oleson, K.W. et al., 2008. Improvements to the Community Land Model and their impact on the hydrological cycle. Journal of Geophysical Research, 113(G1).
Oleson, K.W. et al., 2010. Technical description of version 4.0 of the Community Land Model (CLM), National Center for Atmospheric Research, Boulder, CO, USA.
Peak, D. and Mott, K.A., 2011. A new, vapour-phase mechanism for stomatal responses to

humidity and temperature. Plant, Cell & Environment, 34(1): 162-178.
Pennington, R.T., Lavin, M. and Oliveira, A., 2009. Woody Plant Diversity, Evolution, and Ecology in the Tropics: Perspectives from Seasonally Dry Tropical Forests, Annual Review of Ecology Evolution and Systematics. Annual Review of Ecology Evolution and Systematics, pp. 437-457.
Pennington, R.T., Prado, D.E. and Pendry, C.A., 2000. Neotropical seasonally dry forests and Quaternary vegetation changes. Journal of Biogeography, 27(2): 261-273.
Poulter, B. et al., 2010. Robust dynamics of Amazon dieback to climate change with perturbed ecosystem model parameters. Global Change Biology, 16(9): 2476-2495.
Quesada, C.A. et al., 2012. Basin-wide variations in Amazon forest structure and function are mediated by both soils and climate. Biogeosciences, 9(6): 2203-2246.
Ratter, J.A., 1992. Transitions between Cerrado and Forest Vegetation in Brazil. In: P.A. Furley, J. Proctor and J.A. Ratter (Editors), Nature and Dynamics of Forest-Savanna Boundaries. Chapman & Hall, London, pp. 417-429.
Restrepo-Coupe, N. et al., 2013. What drives the seasonality of photosynthesis across the Amazon basin? A cross-site analysis of eddy flux tower measurements from the Brasil flux network. Agricultural and Forest Meteorology, 182: 128-144.
Running, S.W. and Coughlan, J.C., 1988. A general model of forest ecosystem process for regional applications I. Hydrologic balance, canopy gas exchange and primary production processes. Ecological Modelling, 42: 125-154.
Schaefer, K. et al., 2008. Combined Simple Biosphere/Carnegie-Ames-Stanford Approach terrestrial carbon cycle model. Journal of Geophysical Research, 113(G3).
Sellers, P.J. et al., 1996. A revised land surface parameterization (SiB2) for atmospheric GCMs. Part I: Model formulation. Journal of Climate, 9: 676-705.
Shuttleworth, W.J., 1988. Evaporation from Amazonian Rainforest. Proceedings of the Royal Society of London, Series B, Biological Sciences, 233(1272): 321-346.
Shuttleworth, W.J., 1991. Insight from Large-Scale Observational Studies of Land Atmosphere Interactions. Surveys in Geophysics, 12(1-3): 3-30.
Sitch, S. et al., 2008. Evaluation of the terrestrial carbon cycle, future plant geography and climate-carbon cycle feedbacks using five Dynamic Global Vegetation Models (DGVMs). Global Change Biology, 14(9): 2015-2039.
Van den Hurk, B.J.J.M., Viterbo, P., Beljaars, A.C.M. and Betts, A.K., 2000. Offline validation of the ERA40 surface scheme, European Centre for Medium-Range Weather Forecasts.
Verbeeck, H. et al., 2011. Seasonal patterns of CO2fluxes in Amazon forests: Fusion of eddy covariance data and the ORCHIDEE model. Journal of Geophysical Research, 116(G2).
Verseghy, D.L., 1991. CLASS - A Canadian Land Surface Scheme for GCMs .1. Soil Model. International Journal of Climatology, 11(2): 111-133.
Victoria, R.L., Martinelli, L.A., Mortatti, J. and Richey, J., 1991. Mechanisms of Water Recycling in the Amazon Basin - Isotopic Insights. Ambio, 20(8): 384-387.
Walker, G.K., Sud, Y.C. and Atlas, R., 1995. Impact of the Ongoing Amazonian Deforestation on Local Precipitation - a Gcm Simulation Study. Bulletin of the American Meteorological Society, 76(3): 346-361.
Werth, D. and Avissar, R., 2002. The local and global effects of Amazon deforestation. Journal of Geophysical Research-Atmospheres, 107(D20).

Zeng, X. and Decker, M., 2009. Improving the numerical solution of soil moisture-based Richards equation for land models with a deep or shallow water table. Journal of Hydrometeorology, 10: 308-319.

Zhan, X., Xue, Y. and Collatz, G.J., 2003. An analytical approach for estimating CO2 and heat fluxes over the Amazonian region. Ecological Modelling, 162(1-2): 97-117.

List of Tables

Table 1. Site characteristics, observational data descriptions and their associated references. Site characteristics are from Restrepo-Coupe et al. (2013) + references therein and de Gonçalves et al. (2013) + references therein, unless otherwise noted. Dry season defined as months where precipitation is less than 100 mm.

		Site Characteristics							Eddy Flux Measurements			Soil Moisture Measurements			
Site Lat/Lon	**Biome type**	**Group** [b]	**Canopy Ht.**	**Precip.**	**Dry Season Length** [d]	**Dry Season Precip.** [d]	**Soil texture** [e]	**Soil depth**	**Years used**	**Freq**	**Tower Ht.**	**Years used**	**Freq**	**Measurement Depths**	**Extrap Depth** [j]
[deg]			[m]	[mm y^{-1}]	[months]	[mm $month^{-1}$]		[m]			[m]			[m]	[m]
K34 2.61S/ 60.21W	Tropical evergreen forest	Equatorial Forest	30-35	2328	2.8	64	clay	> 15	2002 - 2005	Hourly	50	1992 – 1993 [f]	weekly [f]	0.1, then intervals of 0.2 from 0.2 to 3.6 [f]	10.0
K67 2.85S/ 54.97W	Tropical evergreen forest	Equatorial Forest	35-40	1597	6.3	49	clay	> 12	2002 - 2004	Hourly	63	1999 - 2005 [g]	monthly [g]	0.3, 0.5, then intervals of 1.0 from 1.0 to 11.0 [g]	25.0
K83 3.01S/ 54.58W	Selectively logged tropical evergreen forest	Equatorial Forest	35-40	1659	5.0	45	clay	> 12	2001 - 2003	Hourly	64	2002 - 2003 [h]	half-hourly [h]	0.15, 0.30, 0.60, 1.0, 2.0, 3.0, 4.0, 6.0, 10.0 [h]	30.0
BAN (or JAV) 9.82S/ 50.13W	Seasonally flooded forest-savanna ecotone	Transitional Forest	5-18 [a, c]	1680	5.3	27	clay loam	> 3	2004 - 2006	Hourly	40	2004 - 2005 [c]	half-hourly [c]	0.1, 0.2, 0.5, 1.0, 1.5, 2.0 [c]	10.0
RJA 10.08S/ 61.93W	Tropical semideciduous forest	Transitional Forest	30	2342	4.3	36	loamy sand	1.2 - 4.0	2000 - 2002	Hourly	60	1992 - 1993 [f]	weekly [f]	0.1, then intervals of 0.2 from 0.2 to 3.6 [f]	--
PDG (or PEG) 21.62S/ 47.63W	cerrado sensu stricto [a]	Cerrado	5-10	1284	7.0	40	loamy sand	1.0 - 3.5	2001 - 2003	Hourly	21	2001 - 2003 [i]	half-hourly [i]	0.1, 0.2, 0.5, 0.8, 1.0, 1.5, 2.0, 2.5 [i]	--

[a] da Rocha et al. (2009).
[b] This study; see Materials and Methods section.
[c] Borma et al. (2009).
[d] Calculated based on time period listed in 'Years used' from the eddy flux measurements.
[e] USDA texture classification using % sand, % silt, % clay values reported in de Gonçalves et al. (2013).
[f] Hodnett et al. (1995).
[g] Nepstad et al. (2002).
[h] Bruno et al. (2006).
[i] da Rocha et al. (2002), and unpublished data.
[j] This study; the depth to which variations in soil moisture were extrapolated below the deepest soil moisture sensor. See Section 2.4 and Appendix B of the Supplement for details.

Table 2. Summary statistics (intercepts, slopes, coefficient of determination R^2) for the linear regressions shown in Figure 3 of latent heat flux (*LE*) on *LE* + sensible heat flux (*H*) as observed (in **bold**) and modeled for the three site groups. Eq – Equatorial Forest sites, Tr – Transitional Forest sites, Cr – Cerrado site. The slopes of all regressions listed are significantly different from zero ($p < 0.001$).

Observations or model	intercept			slope			R^2		
	Eq	Tr	Cr	Eq	Tr	Cr	Eq	Tr	Cr
Observations	**11**	**4**	**5**	**0.70**	**0.71**	**0.51**	**0.90**	**0.78**	**0.54**
LPJ-1.5m	59	30	30	0.43	0.26	0.36	0.17	0.05	0.31
LPJ-8m	64	85	49	0.49	0.16	0.36	0.28	0.03	0.35
SiB2	19	11	10	0.26	0.17	0.12	0.13	0.03	0.08
SiBCASA	12	22	12	0.62	0.46	0.55	0.83	0.45	0.81
LEAFHYDRO-NWT	10	-2	-50	0.53	0.43	0.67	0.47	0.11	0.27
LEAFHYDRO-WT	9	38	-46	0.56	0.45	0.66	0.72	0.27	0.27
CLM3	48	-11	-30	0.20	0.24	0.44	0.06	0.05	0.21
CLM3.5	-2	-16	25	0.82	0.69	0.38	0.57	0.41	0.34

Table 3. Observed (in boldface) and modeled annual totals, monthly maxima, and the month in which the maximum occurs for the upward capillary flux of groundwater into soil ($Q_{g\uparrow}$) at the three sites presented in Figure 4. "OBS-a" and "OBS-b" refer to the inferred $Q_{g\uparrow}$ flux occurring at the depth of the extrapolated soil moisture and the deepest soil moisture sensor, respectively (see Table 1 and Appendix B of the Supplement).

Observations or model	Total (mm year-1)			Monthly maximum (mm mo-1)			Month of maximum		
	BAN	K67	PDG	BAN	K67	PDG	BAN	K67	PDG
OBS-a	**211**	**24**	**--**	**201**	**13**	**--**	**Nov**	**Jun**	**--**
OBS-b	**229**	**22**	**44**	**204**	**18**	**16**	**Nov**	**Dec**	**Jun**
CLM3.5	14	137	0	14	35	0	Nov	Aug	--
CLM4CN	204	278	10	49	54	3	Aug	Oct	Nov
ISAM	0	0	11	0	0	7	--	--	Nov
LEAFHYDRO-WT	416	92	0	119	26	0	Jul	Oct	--

Table 4. Model benchmarking of the magnitude of transpiration fluxes (E_t) across biomes with respect to vegetation demand for water. Note that mean E_t is not representative of an annual mean (see Methods section 2.5). 'high', 'low', and '√' denote models whose mean values are greater than, less than, or within the observational error (taken as a constant 0.5 mm/day for E_t). The last column evaluates whether models do ('√') or do not ('x') match the observed E_t, while also matching all four observed magnitudes of vegetation demand (columns 1-4).

g_s	T_v	*GPP*	*iWUE*	Model	Mean E_t	Right E_t?	Right E_t, Right demand?
				Equatorial forests (K34, K67, K83)			
low	√	low	√	SIB2	1.92	low	x
low	high	√	high	ED2	2.33	low	x
low	√			HTESSEL	2.47	low	x
low	√	high	high	SSiB2	2.48	low	x
low	√			LEAFHYDRO-NWT	2.53	low	x
low	√			LEAFHYDRO-WT	2.61	low	x
low	high	√	high	CN-CLASS	2.66	low	x
low	√	√	high	ISAM	2.72	low	x
low	low	√	√	SiBCASA	2.99	low	x
√	√	high	√	SiB2-mod	3.18	√	x
low	high	√	high	IBIS	3.19	√	x
low	√	√	high	JULES	3.20	√	x
low	√	√	high	SiB3	3.24	√	x
low	√	high	high	ORCHIDEE	3.36	√	x
√	√	√	√	**NOAH-MP**	**3.54**	√	√
√	√	√	√	**OBS**	**3.59**	√	√
high	√	high	high	CLM3.5	4.07	high	x
high	√	high	√	CLM4-CN	4.29	high	x
				Transitional forest (RJA only)			
low	√			CLM3	1.42	low	x
low	high	low	√	SiB2	1.53	low	x
low	high	low	√	ED2	2.22	low	x
low	√	high	high	SSiB2	2.89	low	x
√	high	low	√	JULES	3.00	low	x
low	high			LEAFHYDRO-NWT	3.03	low	x
√	√			HTESSEL	3.04	low	x
low	high	√	high	IBIS	3.04	low	x
low	high			LEAFHYDRO-WT	3.19	low	x
low	high	√	high	CN-CLASS	3.20	low	x
low	√	√	√	ISAM	3.27	√	x
low	√	√	√	SiBCASA	3.45	√	x
√	√	√	√	**OBS**	**3.73**	√	√
√	√	√	√	**CLM4-CN**	**3.86**	√	√
√	√	√	√	**NOAH-MP**	**4.01**	√	√
√	√	√	√	**SiB3**	**4.01**	√	√
√	high	high	√	SiB2-mod	4.18	√	x
√	√	high	√	ORCHIDEE	4.46	high	x
√	√	high	√	CLM3.5	4.58	high	x
				Cerrado (PDG)			
low	√	low	low	SiB2	0.61	low	x
low	√	low	low	CN-CLASS	1.07	low	x
√	√			CLM3	1.09	low	x
√	√	high	√	SiB2-mod	1.34	low	x
√	high	√	high	NOAH-MP	1.44	low	x

√	√	high	high	ED2	1.92	√	x
√	√	√	√	**CLM4-CN**	1.95	√	√
√	√	√	high	CLM3.5	2.00	√	x
√	√			**LEAFHYDRO-NWT**	**2.06**	√	√
√	high	high	high	SSiB2	2.08	√	x
√	√			**LEAFHYDRO-WT**	**2.12**	√	√
√	√	√	√	ISAM	2.13	√	x
√	√	√	√	**OBS**	**2.18**	√	√
√	high	high	√	SiB3	2.29	√	x
√	√			**HTESSEL**	**2.51**	√	√
√	√	high	high	SiBCASA	2.51	√	x
√	√	high	high	ORCHIDEE	2.62	√	x
√	√	high	high	IBIS	3.31	high	x
high	low	high	√	JULES	3.57	high	x

1152

List of Figure Captions

Fig. 1. Mean seasonal climatology (precipitation; P, net radiation; R_n, and evapotranspiration; E) in equivalent water flux units (mm month^{-1}) based on pooled monthly time series data from multiple sites grouped by (a) equatorial forests (K34, K67, K83 sites), (b) transitional forests (RJA, BAN sites), and (c) Cerrado (PDG site). Maps display d) mean monthly precipitation (mm month^{-1}) or e) number of dry season months. Boxes around grouped sites match those around corresponding water flux figures.

Fig. 2. Modeled (colored lines or symbols) and observed (black points & error bars) mean seasonal cycle of E based on monthly time series data averaged (+/- 1 standard deviation) across multiple sites grouped by a) equatorial forest (K34, K67, K83), b) transitional forest (RJA and BAN) and **c)** Cerrado/savanna (PDG). For a) and b), error bars incorporate inter-site and interannual variability, wheareas for c), error bars represent interannual variability only. Gray shaded region denotes dry season (months where precipitation < 100 mm).

Fig. 3. Scatterplots and least squares linear regression of daily values of dry season LE versus $LE + H$ for a) observations and b) – i) select models (see main text for model selection criteria and justification of choice of $LE + H$ as x-axis variable). Deep roots are implemented in the model developments from b) -> c) and d) -> e); groundwater is implemented in model developments from f) -> g) and h) -> i). Data for equatorial and transitional forests were pooled, not averaged, across sites

Fig. 4. Observed (top row) and modeled (bottom two rows) monthly averages of the seasonality of net radiation (R_n), precipitation (P), evapotranspiration (E), total runoff ($Q_s + Q_{sb}$), and the influx of groundwater ($Q_{g\uparrow}$) for three sites. Soil moisture storage (positive) or depletion (negative) is given by the difference between the top of largest of the two lines (P or $P + Q_{g\uparrow}$) and the top of the stacked bars. Contrasting predictions due to shallow vs. deep roots are shown in the middle row; contrasting predictions due to absence vs. presence of groundwater interaction are in the bottom row. Red upward arrow denotes influx of groundwater into the system.

Fig. 5. Modeled (colored lines) and observed (points +/- 1 s.d.) seasonal cycles of a) – c) transpiration (E_t) and d) – f) canopy stomatal conductance (g_s) at one site each of equatorial forests (K67), transitional forests (RJA), and Cerrado (PDG). g): Modeled (colored lines) and observed (solid black line) canopy stomatal conductance normalized by its seasonal maximum ($g_s / g_{s\,max}$) at the K67 site to emphasize seasonality. Inset in g): 1-month lagged seasonal cycle of observed g_s regressed on observed LAI at the K67 site. See main text for methods of estimating E_t from eddy flux measures of E, and for estimating g_s. Models shown for the 3 sites in represent those at each site which simulated well the seasonality and magnitude of E_t. Gray shaded regions denote months where precipitation < 100 mm.

Fig. 6. Probability density of daytime canopy temperature (T_v) at one site each of a) equatorial forests (K67), b) transitional forests (RJA), and c) Cerrado (PDG) where canopy stomatal conductance was estimated. Observations are in black (dashed line is air temperature; solid line is the canopy aerodynamic temperature estimated from the inversion of sensible heat and aerodynamic fluxes). Colored arrows denote models (IBIS at K67 and LEAFHYDRO at RJA) which otherwise well simulate the magnitude of transpiration (E_t) but which have warm canopy

temperature biases.

Fig. 7. Observations ("OBS") and models plotted in intrinsic water use efficiency (*iWUE*) – gross primary production (*GPP*) plot space with text color corresponding to modeled E_t relative to observed E_t , where red (blue) models underestimate (overestimate) E_t by at least 0.5 mm/day. *iWUE* and *GPP* are the mean values observed or predicted for each site. Box represents observational error, which for iWUE is estimated as the inverse of the slopes of the 25th and 75th quantile regressions of $g_s \sim GPP*(h/c_a)$. *GPP* error estimated as +/- 1 standard deviation.

List of Appendices

Appendix A: List of symbols, definitions, and units used in the paper (**Table A1**) and descriptions of the soil hydrology (**Table A2**) and stomatal conductance (**Table A3**) sub-model components for all LBA-DMIP models.

Appendix B: Full description of the methods used to obtain composite seasonal cycles of ΔS_s

Appendix C: A version of Figure 3 in main text which includes the entire set of LBA-DMIP models.

Appendix D: Figure sets encompassing all sites and the entire set of models for the water budget analysis given in Figures 4 of the main text.

Figure 1

Click here to download high resolution image

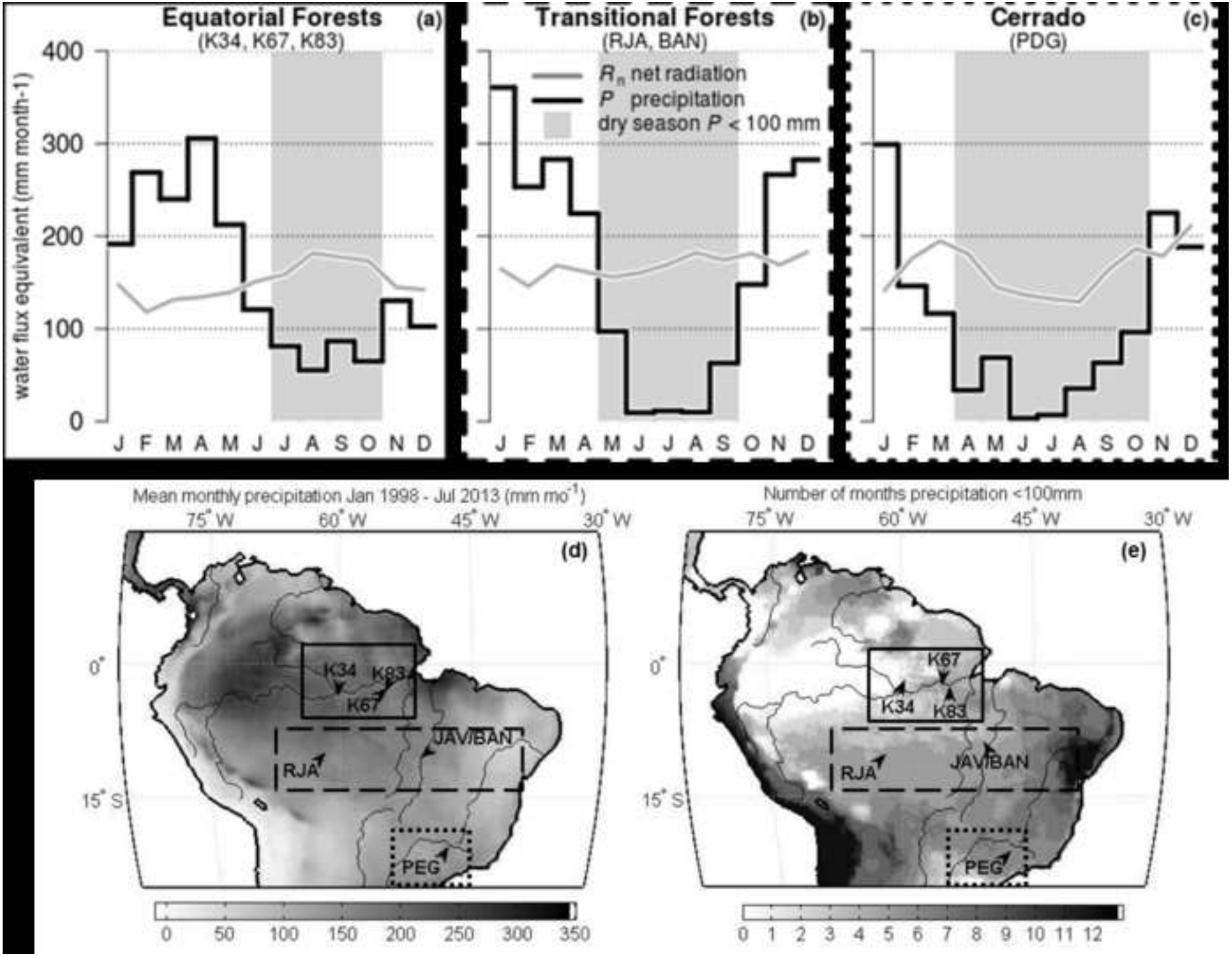

Figure 2

Click here to download high resolution image

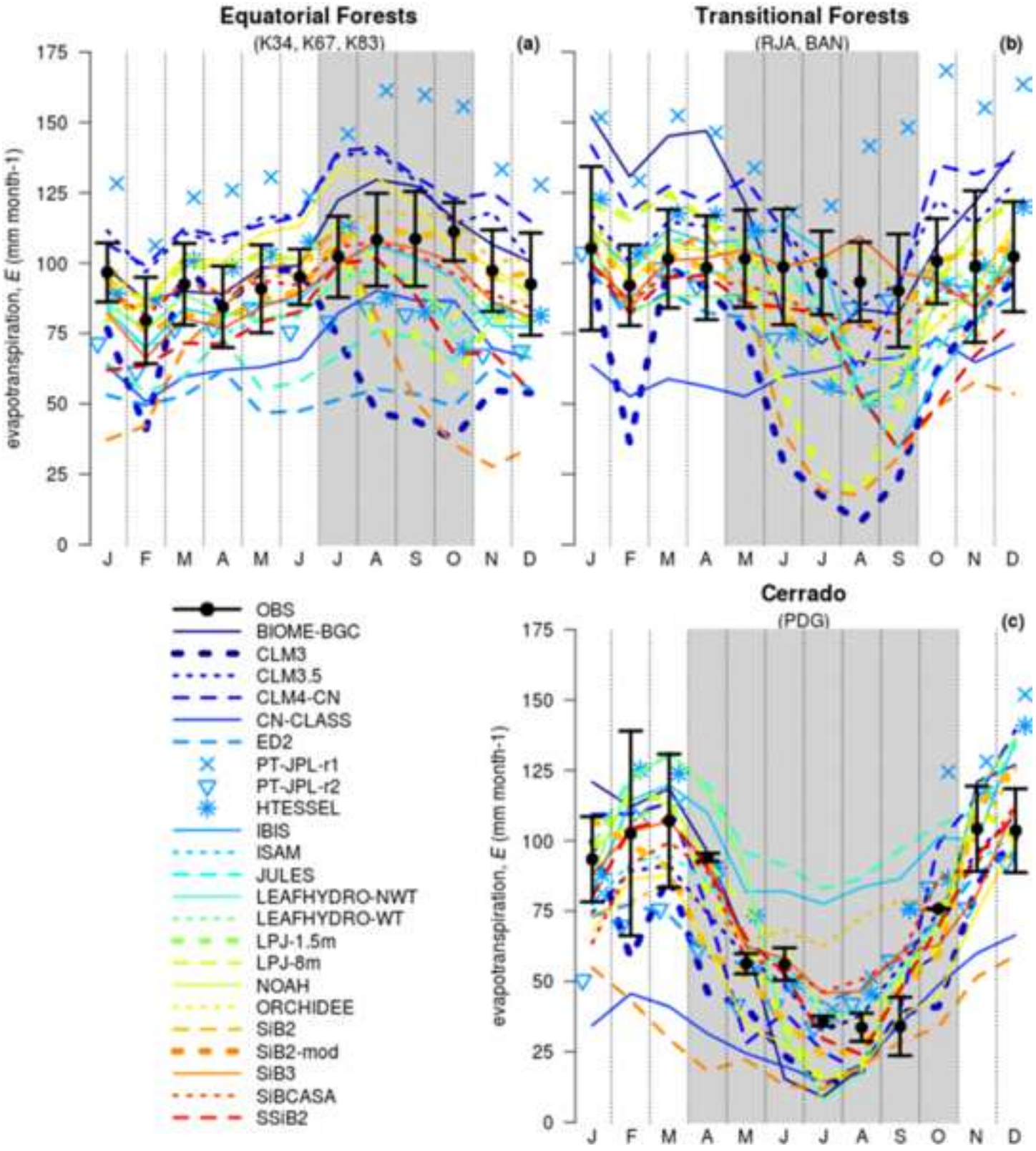

Figure 3

Click here to download high resolution image

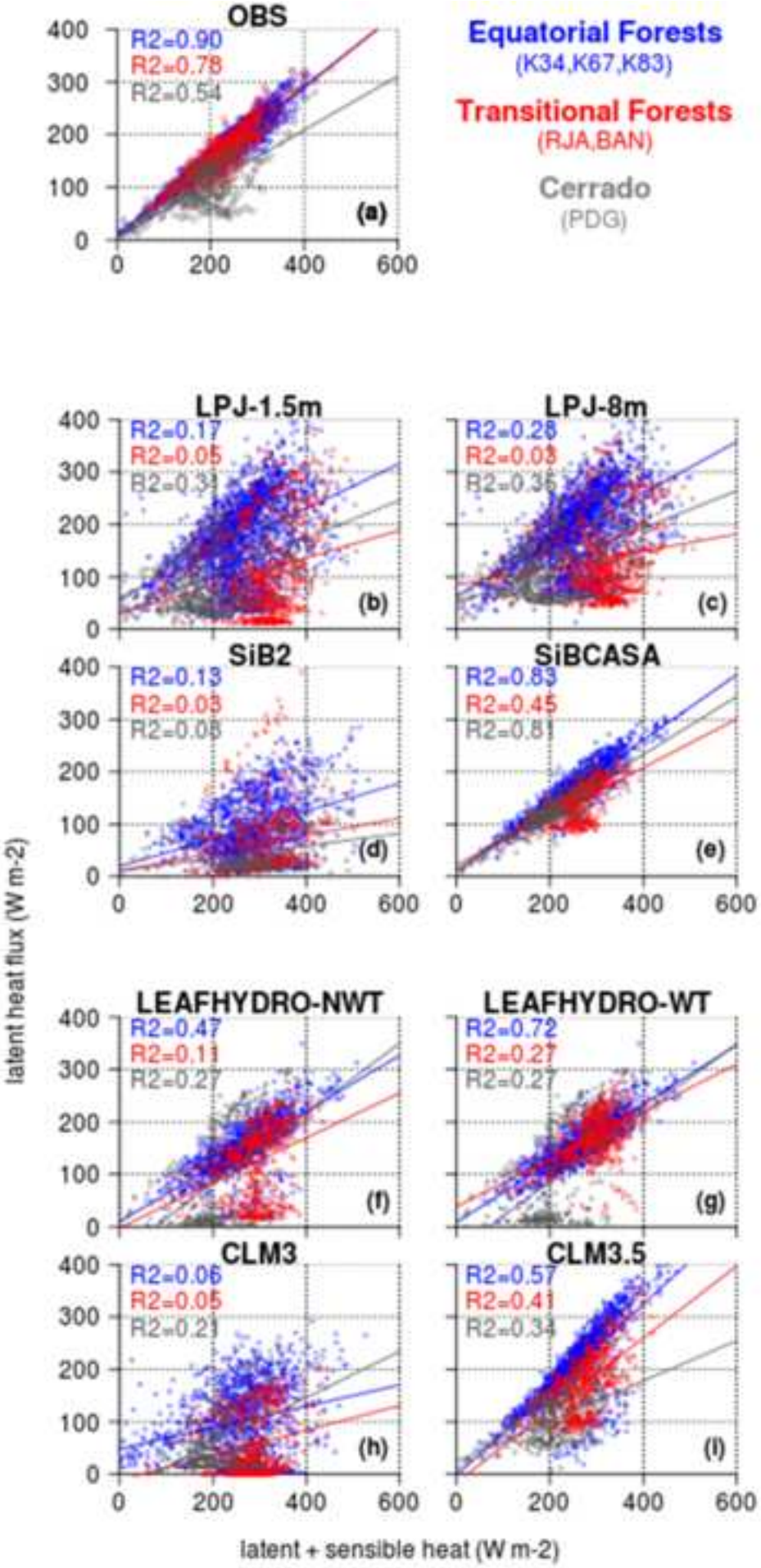

Figure 4

Click here to download high resolution image

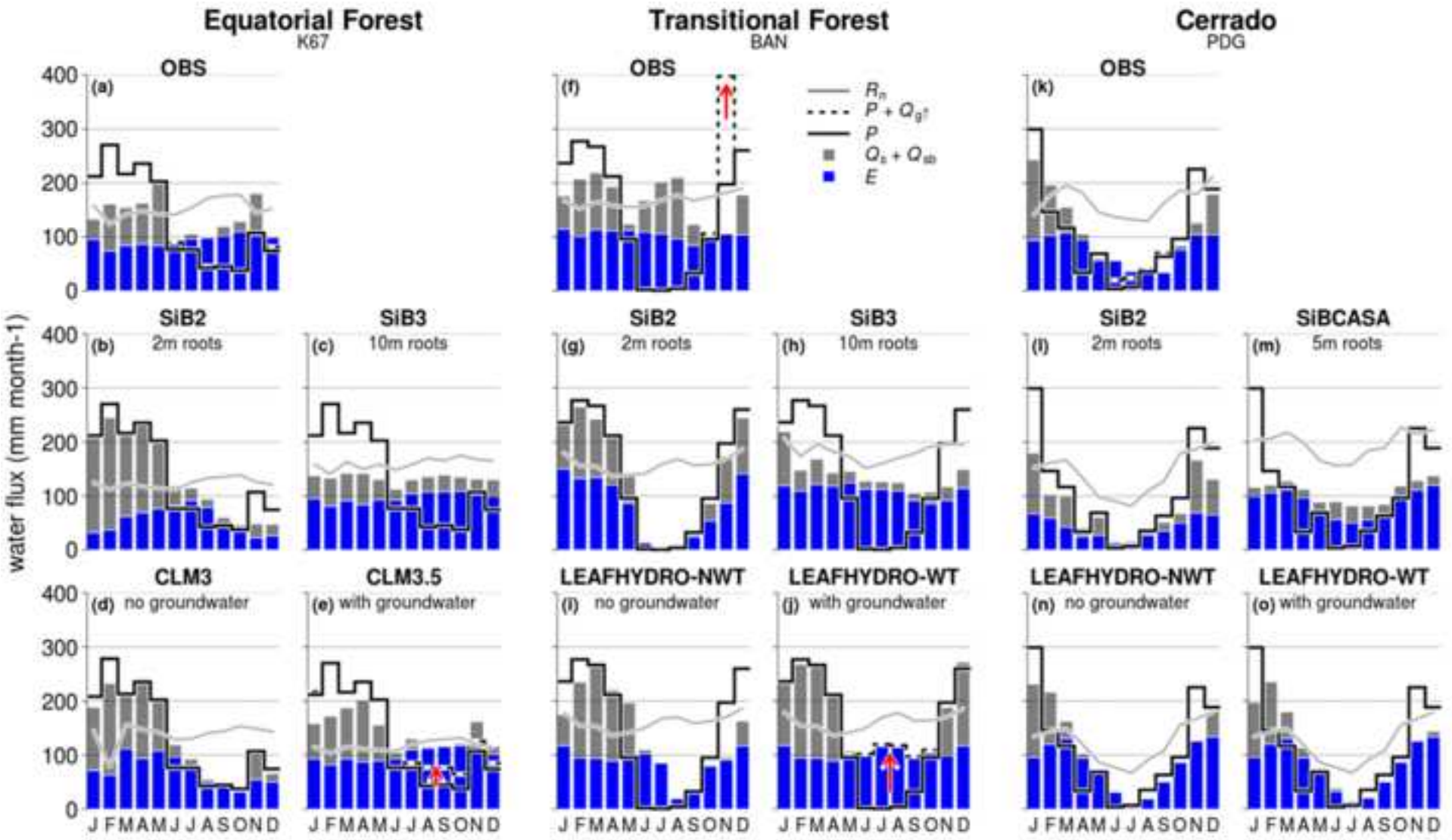

Figure 5

Click here to download high resolution image

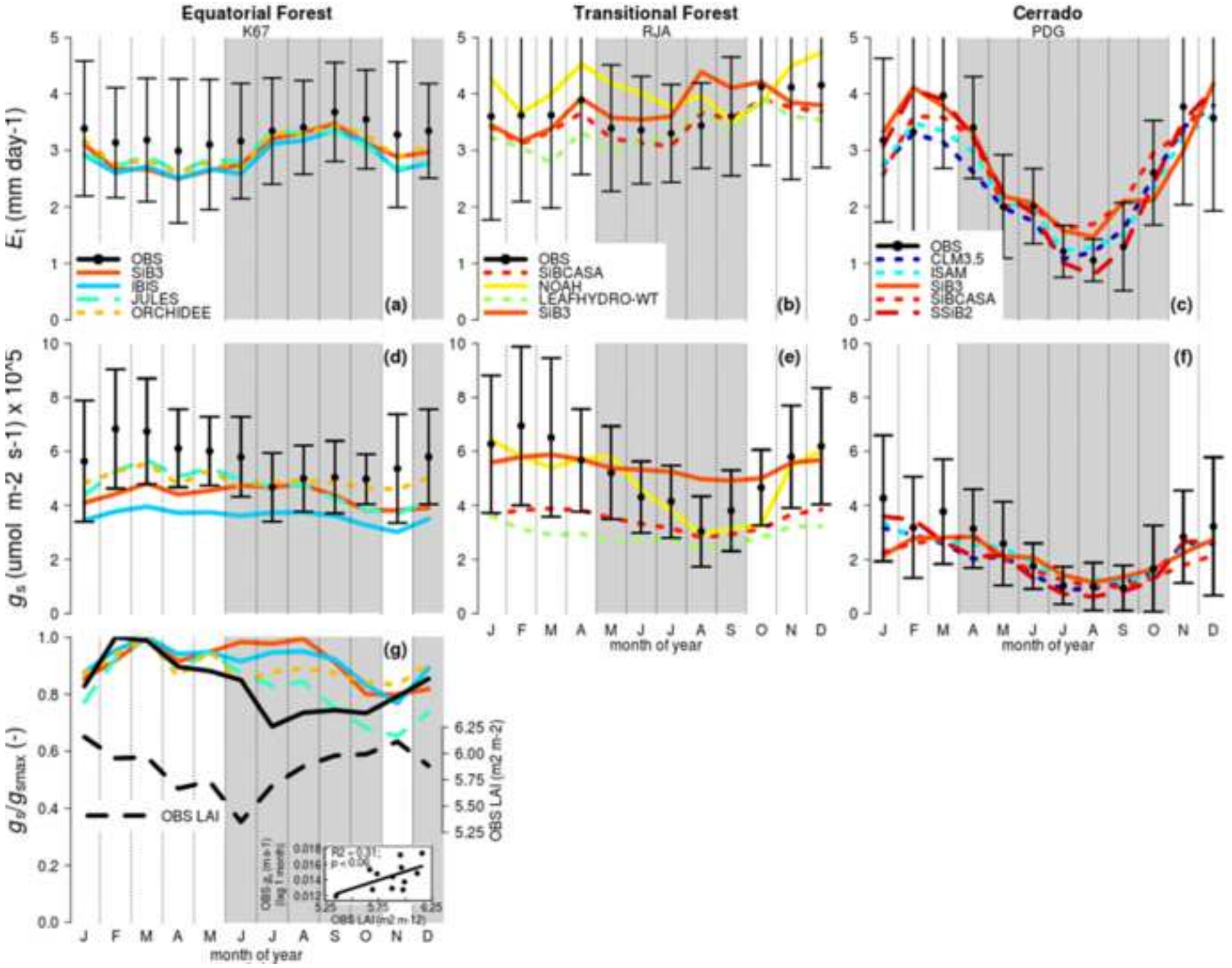

Figure 6

Click here to download high resolution image

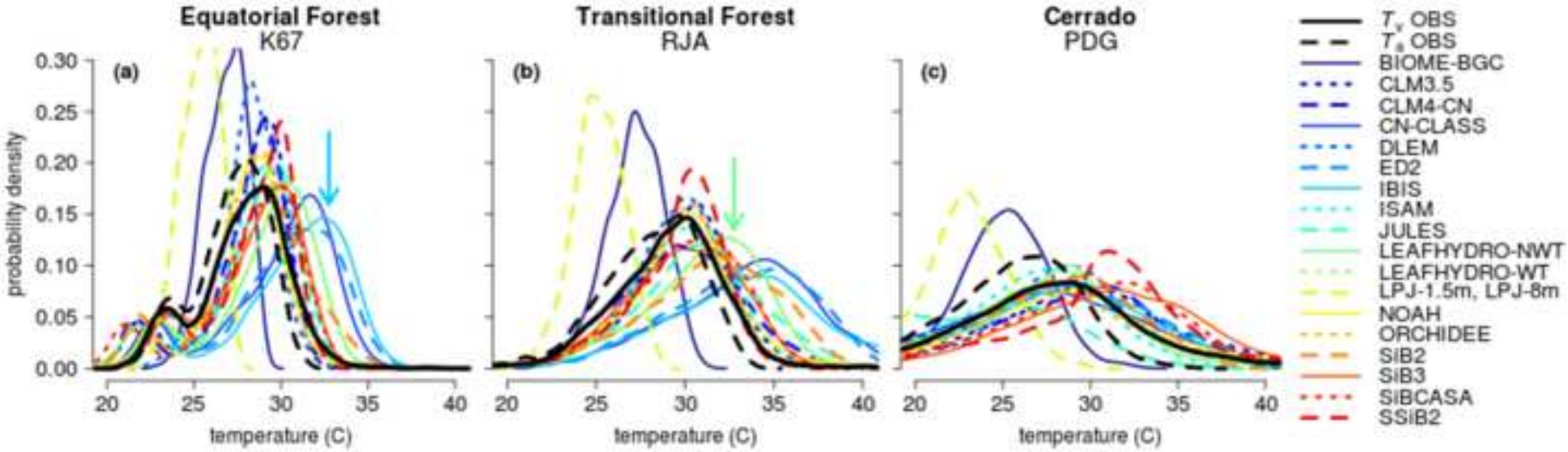

Figure 7

Click here to download high resolution image

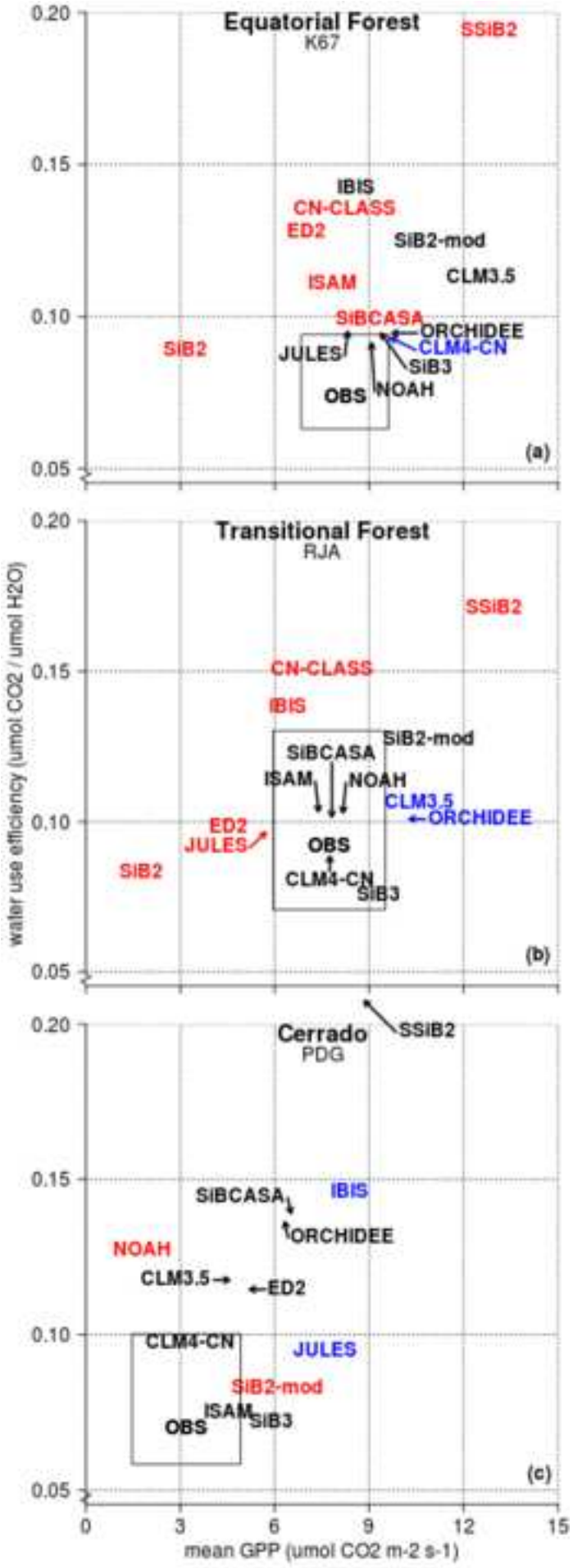

Appendix A: List of symbols, definitions, and units used in the paper (**Table A1**) and descriptions of the soil hydrology (**Table A2**) and stomatal conductance (**Table A3**) sub-model components for all models.

Table A1. List of symbols, definitions, and units used in the paper.

Symbol	Definition	Instantaneous Units	Aggregated units
	stand-level water budget		
P	precipitation	kg m^{-2} s^{-1}	mm $month^{-1}$
E	total evapotranspiration	kg m^{-2} s^{-1}	mm $month^{-1}$
E_t	transpiration	kg m^{-2} s^{-1}	mm $month^{-1}$
E_i	evaporation from canopy interception	kg m^{-2} s^{-1}	mm $month^{-1}$
E_s	soil evaporation	kg m^{-2} s^{-1}	mm $month^{-1}$
Q_t	Q_s + Q_{sb} (positive out of system) less any $Q_{g\uparrow}$	kg m^{-2} s^{-1}	mm $month^{-1}$
Q_s	surface runoff	kg m^{-2} s^{-1}	mm $month^{-1}$
Q_{sb}	subsurface drainage to streams and groundwater	kg m^{-2} s^{-1}	mm $month^{-1}$
$Q_{g\uparrow}$	upward capillary flux or lateral transport from groundwater	kg m^{-2} s^{-1}	mm $month^{-1}$
ΔS_i	change in stored canopy interception	kg m^{-2}	mm $month^{-1}$
ΔS_o	change in stored open water	kg m^{-2}	mm $month^{-1}$
ΔS_s	change in stored soil moisture	kg m^{-2}	mm $month^{-1}$
	stand- and leaf-level energy & carbon fluxes		
R_n	net all-wave radiation flux density	W m^{-2}	W m^{-2}
R_s	total downward shortwave radiation flux density	W m^{-2}	W m^{-2}
R_p	photosynthetically active photon flux density	µmol m^{-2} s^{-1}	µmol m-2 s-1
LE	latent heat flux	W m^{-2}	W m^{-2}
H	sensible heat flux	W m^{-2}	W m^{-2}
GPP	stand-level gross photosynthesis	µmol CO_2 m^{-2} s^{-1}	µmol CO2 m^{-2} s^{-1}
g_s	stand-level canopy stomatal conductance	mm s^{-1} or µmol m^{-2} s^{-1}	mm s^{-1} or µmol m^{-2} s^{-1}
r_b	aerodynamic resistance	s m^{-1}	s m^{-1}
A	leaf-level gross photosynthesis	µmol CO2 m^{-2} s^{-1}	µmol CO2 m^{-2} s^{-1}
A_n	leaf-level net photosynthesis (gross minus leaf dark respiration)	µmol CO2 m^{-2} s^{-1}	µmol CO2 m^{-2} s^{-1}
	atmospheric state variables or constants		
c_a	atmospheric CO2 concentration	mole fraction	mole fraction
T_a	atmospheric air temperature	K	K
ρ_a	atmospheric air density	kg m^{-3}	kg m^{-3}
u	magnitude of horizontal wind speed	m s^{-1}	m s^{-1}

u_*	friction velocity	$m\ s^{-1}$	$m\ s^{-1}$
c_p	specific heat of dry air at constant pressure	$J\ K^{-1}$	
Δ	slope of equilibrium saturation vapor pressure curve	$kPa\ K^{-1}$	
γ	psychrometric constant	$kPa\ K^{-1}$	
λ	latent heat of vaporization	$J\ kg^{-1}$	
	soil state variables		
ψ	soil matric potential	Pa	Pa
ϑ	volumetric soil moisture content	$m^3\ m^{-3}$	$m^3\ m^{-3}$
	vegetation state variables		
T_v	vegetation temperature	K	K
h	relative humidity	%	%
D	vapor pressure deficit relative to T_v	Pa	Pa
LAI	leaf area index	$m^2\ m^{-2}$	$m^2\ m^{-2}$
c_s	canopy air space CO2 concentration	mole fraction	mole fraction
c_i	internal leaf CO2 concentration	mole fraction	mole fraction
Γ	CO2 compensation point for C3 plants	mole fraction	mole fraction
m	Ball-Berry slope	(-)	(-)

Table A2. Soil model characteristics and rooting depth for participating LBA-DMIP models, grouped by bottom flow condition (e.g., free drainage versus aquifer), then by soil depth. Note that for some models, soil depth does not equate to rooting depth at all sites (LEAFHYDRO, SiB3, SiBCASA, SiB2-mod); soil depth is given for each model in Appendix D. "Eq. Forests" refer to the following sites: K34, K67, K83; "Trans. Forests" are RJA, BAN; "Cerrado" is PDG. Relevant reference is specific to description of soil hydrology model and may differ from general model references listed in de Gonçalves et al. in press. Models in bold italic are selected models reported in Figure 4 of the main text.

Model name	Pedotransfer model	Bottom flow condition	Rooting depth Eq. Forests	Rooting depth Trans. Forests	Rooting depth Cerrado	Number soil layers	Relevant reference
		shallow soil depths (< 3.5 m) and no aquifer					
LPJ-1.5m	N/A	drainage + saturation excess	1.5 m	1.5 m	1.5 m	2	Gerten et al. (2004)
SiB2	CH (1978) [a]	standard free drainage + flow from soil moisture heterogeneity	2.0 m	2.0 m	2.0 m	3	Sellers et al. (1996)
LEAFHYDRO-NWT	CH (1978) [a]	standard free drainage	2.0 m	2.0 m	2.0 m	11	Fan and Miguez-Macho (2010)
HTESSEL	CH (1978) [a]	standard free drainage	2.9 m	2.9 m	2.9 m	4	Balsamo et al. (2009)
		intermediate soil depths (3.5 - 5.0 m) and no aquifer					
CLM3.0	CH (1978) [a]	standard free drainage	3.4 m	3.4 m	3.4 m	10	Oleson et al. (2004)
SSiB2	CH (1978) [a]	standard free drainage + flow from soil moisture heterogeneity	3.5 m	3.5 m	3.5 m	3	Sellers et al. (1996)
CN-CLASS	CH (1978) [a]	standard free drainage	4.1 m	4.1 m	4.1 m	3	Verseghy (1991)
		deep soil (> 5.0 m) and no aquifer					
SiBCASA	CH (1978) [a]	standard free drainage + flow from soil moisture heterogeneity	5.0 m	5.0 m	5.0 m	25 [b]	Sellers et al. (1996) [b]
LPJ-8m	N/A	drainage + saturation excess	8.0 m	8.0 m	8.0 m	2	Gerten et al. (2004)

SiB2-mod	CH (1978) [a]	standard free drainage + flow from soil moisture heterogeneity	10.0 m	10.0 m	10.0 m	10 [b]	Sellers et al. (1996) [b]
		variable soil depths and no aquifer					
SiB3	CH (1978) [a]	standard free drainage	10.0 m	5.0 - 10.0 m	3.5 m	10	I. Baker, personal communication
BIOME-BGC	CH (1978) [a]	saturation excess (bucket model)	3.0 - 5.0m	1.0 – 10.0 m	1.0 m	1	Running and Coughlan (1988)
ED2	CH (1978) [a]	standard free drainage	8.0 m	2.0 - 3.0 m	6.0 m	16	N. Levine, personal communication
IBIS	CH (1978) [a]	standard free drainage	8.0 m	4.0 - 8.0 m	4.0 m	6	Foley et al. (1996)
JULES	CH (1978) [a]	standard free drainage	8.0 m	2.0 - 3.0 m	6.0 m	4	Best et al. (2011)
ORCHIDEE	N/A	saturation excess (variable bucket depth model)	10.0 m	2.0 – 4.0 m	2.0 m	2	Ducoudre et al. (1993); de Rosnay and Polcher (1998)
		shallow/intermediate soil depths (< 5.0 m) and unconfined aquifer					
NOAH-MP	CH (1978) [a]	2-way flow using depth to water table and unconfined aquifer (SimGM)	2.0 m	2.0 m	2.0 m	4	Niu et al. (2011)
CLM3.5	CH (1978) [a]	2-way flow using depth to water table and unconfined aquifer	3.4 m	3.4 m	3.4 m	10	Oleson et al. (2008)
CLM4-CN	CH (1978) [a]	2-way flow using depth to water table and unconfined aquifer	3.4 m	3.4 m	3.4 m	10	Oleson et al. (2010)
ISAM	CH (1978) [a]	2-way flow using depth to water table and unconfined aquifer	3.4 m	3.4 m	3.4 m	10	Oleson et al. (2008)
LEAFHYDRO-WT	CH (1978) [a]	2-way flow using depth to water table and unconfined aquifer	2.0 m	2.0 m	2.0 m	14	Fan and Miguez-Macho (2010)
		stand-alone ET model with no soil sub-model					
PT-JPL-r1 [c]	N/A	N/A	N/A	N/A	N/A	N/A	Fisher et al. (2009)

PT-JPL-r2 [c]	N/A	N/A	N/A	N/A	N/A	N/A	Fisher et al. (2009)	

[a] Refers to Clapp and Hornberger (1978)

[b] 3 groups of soil layers remain as described in Sellers et al. (1996) (surface layer, rooting layer, bottom layer) as are relevant fluxes, but number of rooting layers is increased.

[c] r1 and r2 refer to different schemes for estimating net radiation (R_n). See Fisher et al. (2009) for further details.

Table A3. Participating models and associated conductance models and parameter values, grouped by closure equation enabling solution of g_s.

Model name	Time step	*gs* model	closure equation	relevant parameter values for broadleaf evergreen forests	Implementation reference
			Jarvis-type (photosynthesis not simulated)		
HTESSEL	Hourly	J76	$g_s = LAI*g_{smax}*f3(R_s)*f4(\theta)*f5(D)$	g_{smax} = dependent on vegetation type $f3(R_s) = 0.81(1 + 0.004*R_s)/(0.004*R_s + 0.05)$ (R_s in W m-2) $f4(\theta) = (\theta - 0.171)/(0.323 - 0.171)$; $\theta = \Sigma_k(R_k*\theta_k)$; θ_k = moisture content layer k (m3/m3); R_k = root content layer k $f5(D) = \exp(-0.0003*D)$; (D in Pa)	Van den Hurk et al. (2000)
LEAFHYDRO-NWT	Hourly	J76	$g_s = g_{smax}*f1(T_v)*f2(T_v)*f3(R_s)*f4(\psi)*f5(D)$	g_{smax} = 10 mm/s $f1(T_v) = 1/(1 + \exp(-0.26*(T_v - 281.5)))$ $f2(T_v) = 1/(1 + \exp(0.124*(T_v - 310.1)))$ $f3(R_s) = 1/(1 + \exp(-0.047*(R_s - 196)))$ $f4(\psi) = 1/(1 + \exp(-7.42e6*(\psi + 1.07e6)))$ (ψ negative) $f4(D) = 1/(1 + \exp(0.0051*(D - 4850)))$	Model source code
LEAFHYDRO-WT	Hourly	J76	same as LEAFHYDRO-NWT	same as LEAFHYDRO-NWT	Model source code
			Jarvis-type (with photosynthesis)		
BIOME-BGC	Daily	J76	$g_s = g_{smax}*f1(T_v)*f3(R_p)*f4(\psi)*f5(D)$	g_{smax} = 6 mm s-1 $f1(T_v) = (T_v - 281)/(273 - 281)$ $f3(R_p) = R_p/(75 + R_p)$ $f4(\psi) = (\psi - 2.2)/(0.34 - 2.2)$ $f5(D) = (D - 3600)/(1100 - 3600)$	Golinkoff (unpublished)
			assume constant ci/ca under non-water stressed conditions (with photosynthesis)		
LPJ-1m	Daily	M95, HP96	$g_s = g_{smin} + 8*A$ (non-water stressed) $g_s = -g_m*\ln(1 - E_{supply}/(E_{pot})$ (water stressed)	g_{smin} = 0.5 mm s-1 g_m = 5 mm s-1	Sitch et al. (2003)
LPJ-8m	Daily	M95, HP96	same as LPJ-1m	same as LPJ-1m	Sitch et al. (2003)
			Leuning-type		

ED2	Hourly	L95	$g_s = g_{smin} + m*A/((c_s - \Gamma)(1 + D/D_0)$	m = 8	Medvigy et al. (2009)
IBIS	Hourly	L95	$g_s = g_{smin} + m*A/((c_s - \Gamma)(1 + D/D_0)$	g_{smin} = 0.01 mm s-1; m = 8	Foley et al. (1996)
CN-CLASS	Hourly	L95	$g_s = g_{smin} + m*A/((c_s - \Gamma)(1 + D/D_0)$	m = 6; D_0 = 1500	
JULES	Hourly	J94	$g_s = g_{smin} + m*A/((c_s - \Gamma)(1 + D/D_0)$	m = 12.8; D_0 = 0.013	Clark et al. (2011)
			Ball-Woodrow-Berry-Collatz-type		
SiB2-mod	Hourly	BWBC	$g_s = g_{smin} + m*A_n/c_s*h$		
SiB2	Hourly	BWBC	$g_s = g_{smin} + m*A_n/c_s*h$	g_{smin} = 0.01 mm s-1; m = 9	Sellers et al. (1996)
SiB3	Hourly	BWBC	$g_s = g_{smin} + m*A_n/c_s*h$	g_{smin} = 0.01 mm s-1; m = 9	Sellers et al. (1996)
SiBCASA	Hourly	BWBC	$g_s = g_{smin} *L + m*A_n/c_s*h$	m = 9	Schaefer et al. (2008)
SSiB2	Hourly	BWBC	$g_s = g_{smin} + m*A_n/c_s*h$	g_{smin} = 0.01 mm s-1; m = 9	Zhan et al. (2003)
CLM3.0	Hourly	BWBC	$g_s = g_{smin} + m*A/c_s*h$	g_{smin} = 0.05 mm s-1; m = 9	Oleson et al. (2004)
CLM3.5	Hourly	BWBC	$g_s = g_{smin} + m*A/c_s*h$	g_{smin} = 0.05 mm s-1; m = 9	Oleson et al. (2004)
CLM4-CN	Hourly	BWBC	$g_s = g_{smin} + m*A/c_s*h$	g_{smin} = 0.05 mm s-1; m = 9	Oleson et al. (2010)
ISAM	Hourly	BWBC	$g_s = g_{smin} + m*A/c_s*h$	g_{smin} = 0.05 mm s-1; m = 9	Oleson et al. (2004)
NOAH-MP	Hourly	BWBC	$g_s = g_{smin} + m*A/c_s*h$		Niu et al. (2011)
ORCHIDEE	Hourly	BWBC	$g_s = g_{smin} + m*A/c_s*h$	g_{smin} = 0.01 mm s-1; m = 9	Krinner et al. (2005)
			stand-alone ET model with no stomatal conductance		
PT-JPL-r1 [a]	Hourly	N/A	N/A	N/A	Fisher et al. (2009)
PT-JPL-r2 [a]	Hourly	N/A	N/A	N/A	Fisher et al. (2009)

[a] r1 and r2 refer to different schemes for estimating net radiation (R_n). See Fisher et al. (2009) for further details.

M95: Monteith (1995)
HP96: Haxeltine and Prentice (1996)
J76: Jarvis (1976)
BWBC (Ball-Woodrow-Berry-Collatz): Ball et al. (1987); Collatz et al. (1991)
L95: Leuning et al. (1995)
J94: Jacobs et al. (1994), Cox et al. (1998)

Appendix B: Methods used to obtain composite seasonal cycles of ΔS_s and supplementary soil moisture figures

Because soil moisture measurements only capture a portion of the total unsaturated zone reservoir, it was necessary to estimate contributions of deep soil moisture to the total soil moisture storage term and thus its seasonality. We used the following method to estimate month-to-month changes in total soil moisture storage (ΔS_s): First, for sites with soil moisture measurements made non-continuously (weekly to monthly), we gap-filled the discrete measurements using linear interpolation (in time) between points, for the purposes of estimating the local minima and maxima and the dates at which they occur each year (Figure B1). In some cases we used a 30-day moving average to aid in picking these points. We found at all sites (except PDG) that the seasonal amplitude (max – min) of soil moisture followed a predictable decay pattern with depth, which we fit using an exponential function Figure B2 a,c,e). Likewise, the timing during the year at which local minima and maxima occurred also predictably increased (in time) with depth, which we fit using linear interpolation (Figure B2 b,d,f). Then, using the extrapolated amplitudes and dates of minima and maxima, we estimated seasonal variations in deep soil moisture beyond the domain of the measurements (Figure B3). Finally, we estimated the month-to-month changes in total soil moisture by integrating over depth and time differencing the monthly means and then averaged over replicate years to end with a composite 12-month seasonal cycle of ΔS_s (Figure B4). We did this last step using both the original and extrapolated set of measurements to assess the contribution of the deep unmeasured soil moisture to the total and found that in most cases it was small.

The seasonal cycle of ΔS_s for all six sites (K34, K67, K83, RJA, BAN, PDG) as determined by this method is shown in Figure B4. Estimation of seasonal changes in soil moisture below the measurement domain was not done for RJA and PDG sites. At PDG, this site did not have a predictable decay pattern of the seasonal amplitude in soil moisture with depth (Fig. B2e), rendering extrapolation impossible. At RJA, the presence of bedrock as shallow as 4m meant extrapolation was unnecessary.

Once the seasonal cycle of ΔS_s was determined, we estimated the seasonal cycle of Q_t as

per Eq. (2) in the main text. For the seasonal cycle of Q_t and all other water budget components at all six sites, see Appendix D.

Appendix B figures

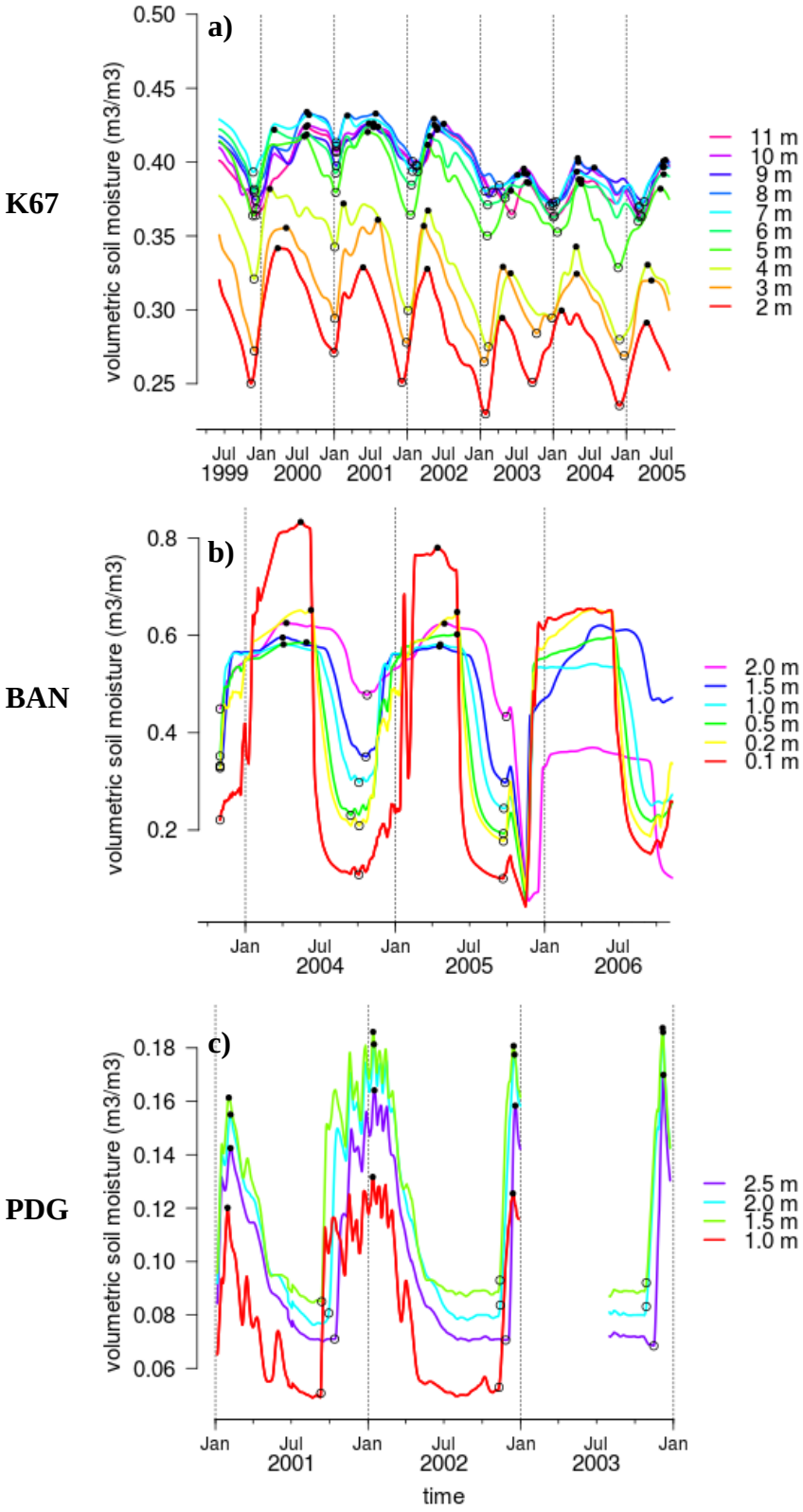

Fig. B1. Measured soil moisture interpolated to a daily timestep with local minima (open circles) and maxima (solid circles) picked at each measurement depth and in each hydrological year for each of the three sites presented in Figs. 4 – 6 in the main text. **a)** Equatorial Forest K67 site, **b)** Transitional Forest BAN site, **c)** Cerrado PDG site.

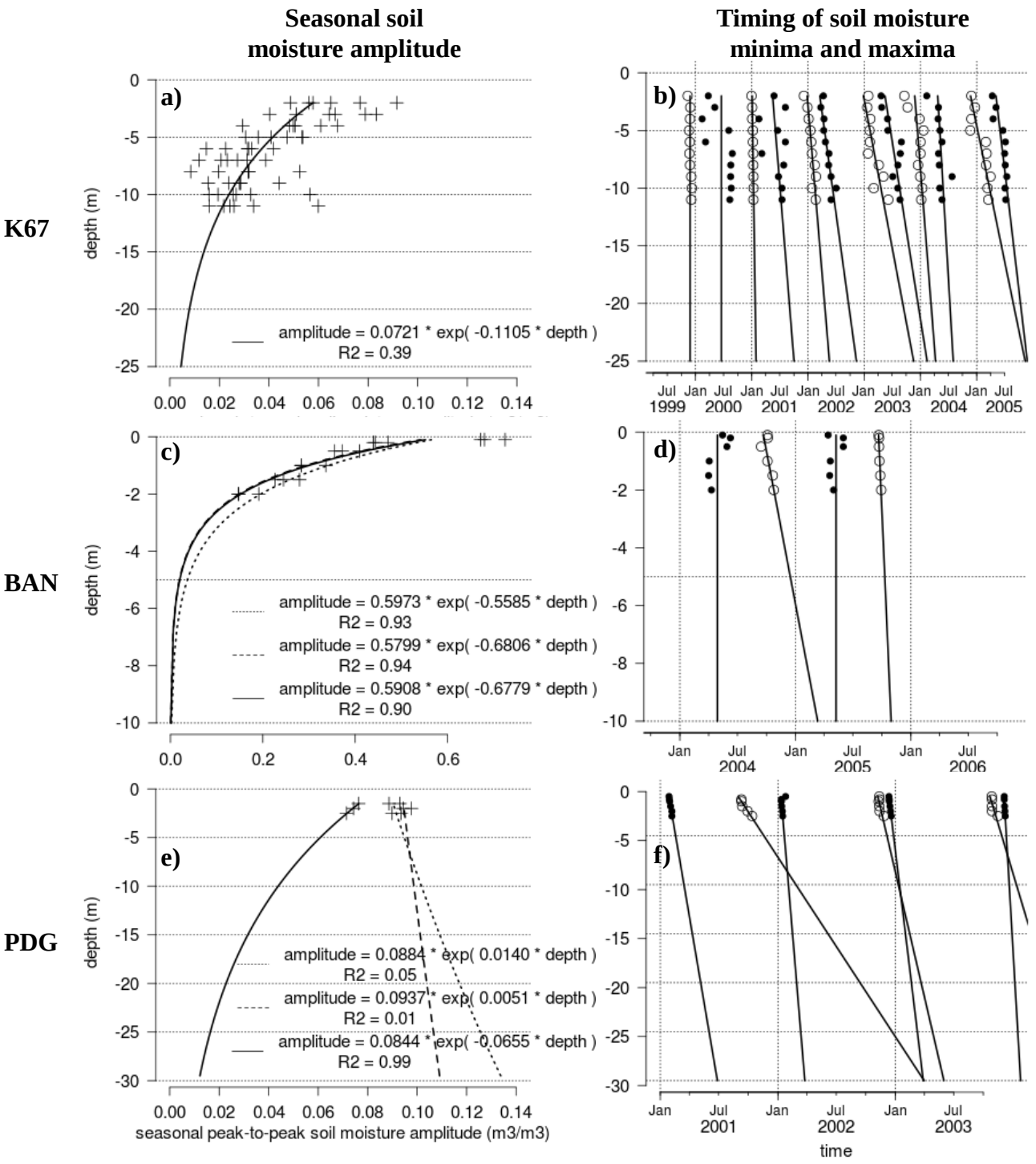

Fig. B2. Extrapolation of soil moisture shown in Fig. B1 beyond measurement domain for each of three sites presented in the main text. Left panels **a)**, **c)**, **e)**: Estimation of the decay in amplitude (soil moisture at maxima less that at minima; selected points shown in Fig. B1) with depth via an exponential fit. Right panels **b)**, **d)**, **e)**: Estimation of timing of maxima of propagating wetting fronts (least-square linear fits to solid circles shown in Fig. B1) and minima of drying fronts (fits to open circles shown in Fig. B1) with depth.

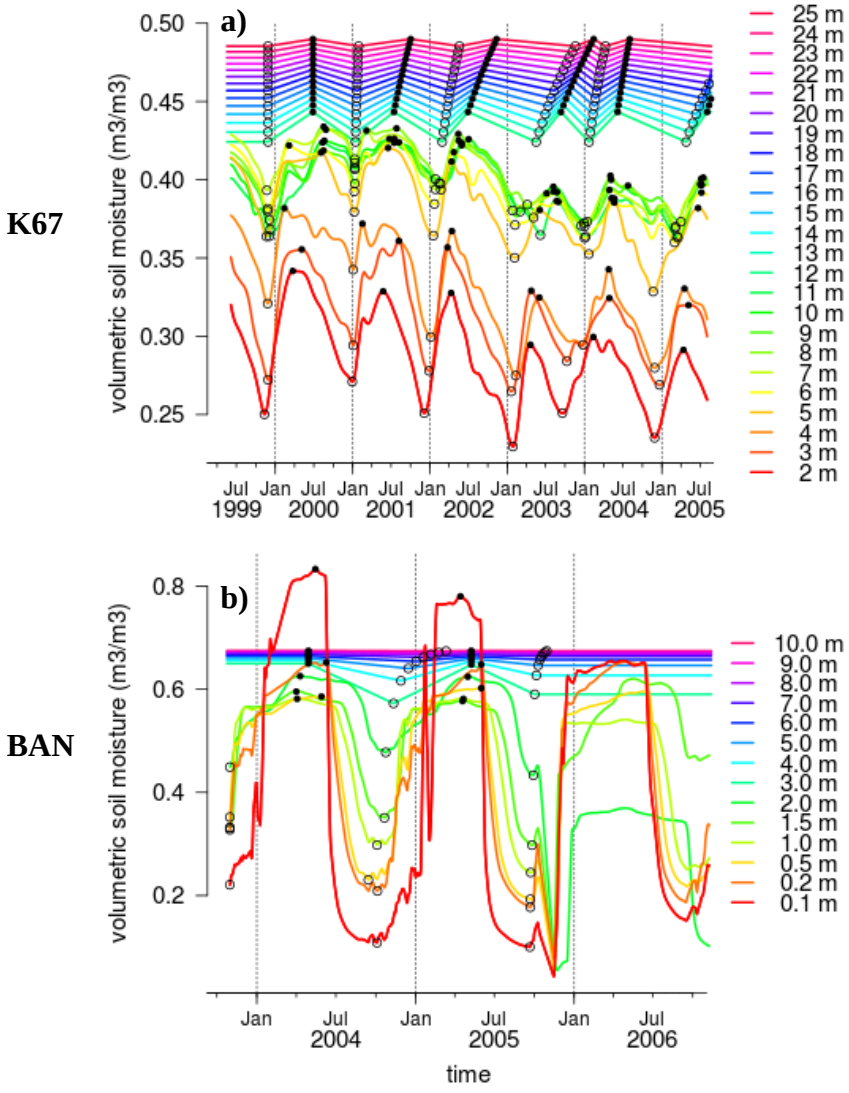

Fig. B3. Extrapolated data together with original measured soil moisture data for **a)** K67 and **b)** BAN sites. Depth extrapolation was not possible for the PDG site due to a lack of a consistent decay pattern of amplitude with depth (Fig. B2e).

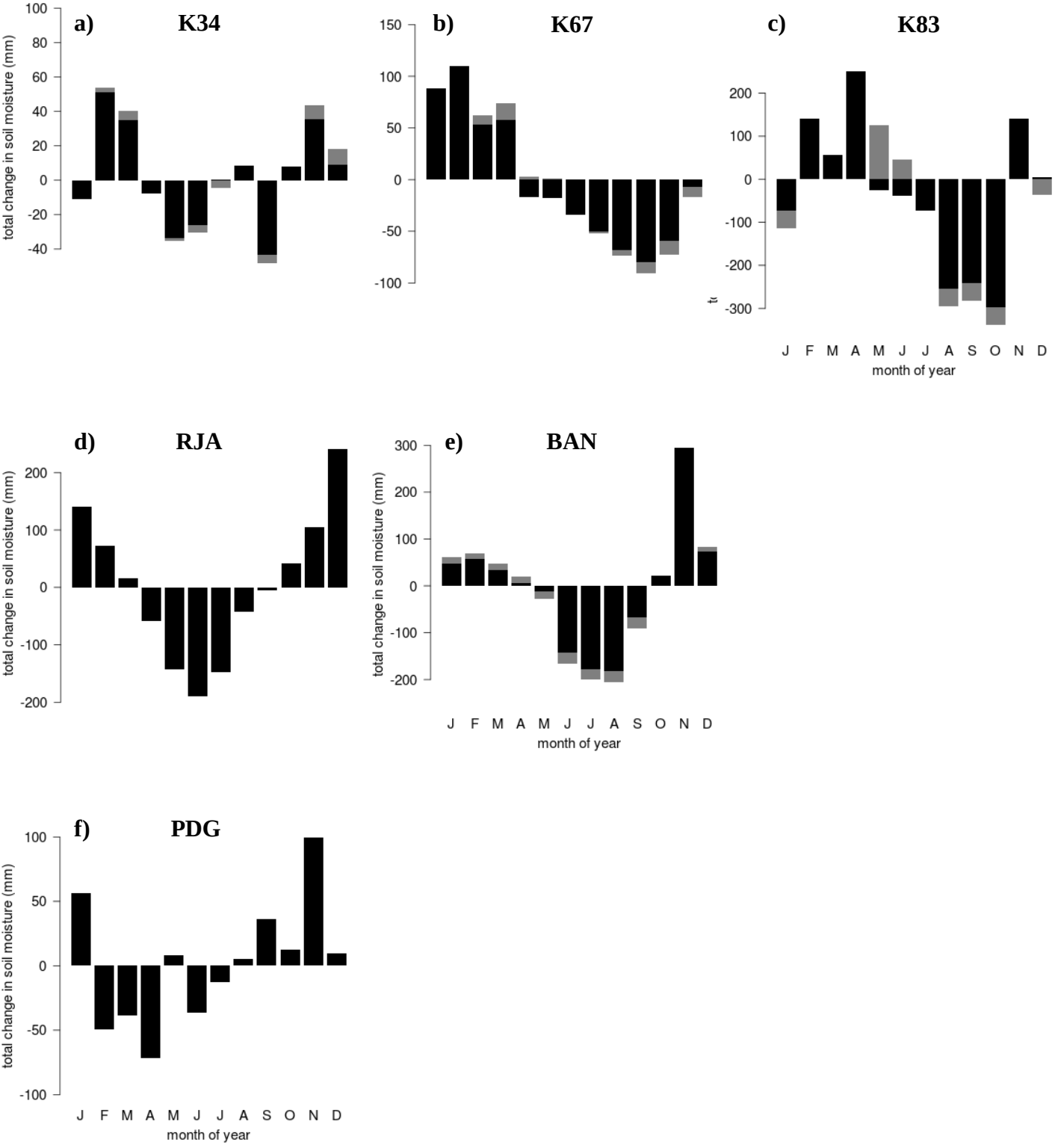

Fig. B4. Seasonal cycle of the change in total soil moisture (ΔS_s), showing contributions from original (black) measured depths and extrapolated (gray) depths for all six sites: Equatorial Forest sites **a)**, **b)** and **c)**, Transitional Forest sites **d)** and **e)**, and Cerrado **f)**. The magnitude of contribution of extrapolated data to seasonal cycle of ΔS_s is governed by the decay of seasonal amplitude with depth (Fig. 2a) and its timing by the mean across years as given in Fig 2b. Note y-axis differences across sites.

Figure C1. Same as Figure 3 (main text), but showing all participating models of the LBA-DMIP (de Gonçalves et al., 2013), grouped by soil depth and presence/absence of an aquifer below the soil domain. Data points for equatorial forests in red, transitional forests in blue, cerrado in gray.

Equatorial forests (K34, K67, K83),
Transitional forests (RJA, BAN)
Cerrado (PDG)

Observations

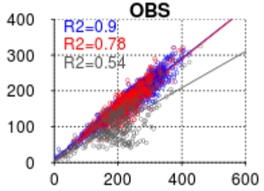

Shallow (< 3.5 m), no aquifer

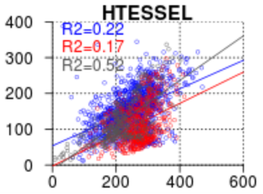

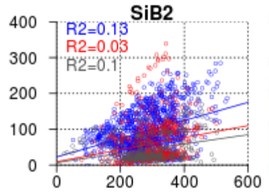

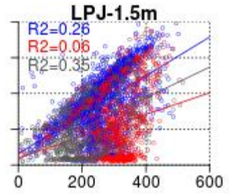

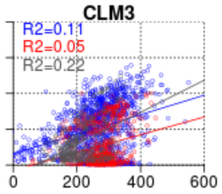

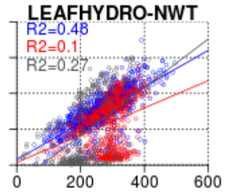

Intermediate (3.5 – 5.0 m), no aquifer

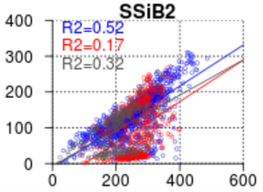

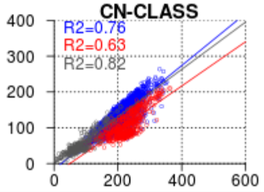

deep roots added

aquifer added

Deep (> 5m), no aquifer

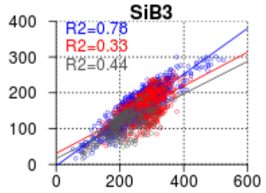

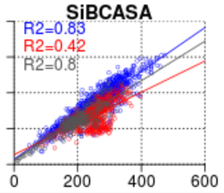

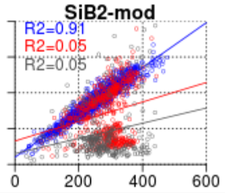

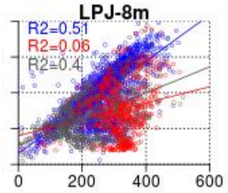

Variable rooting depths

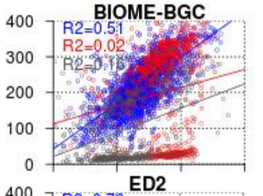

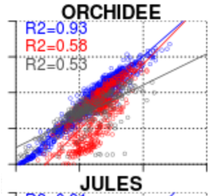

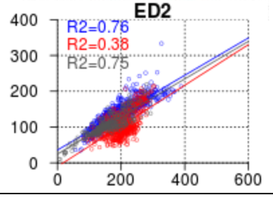

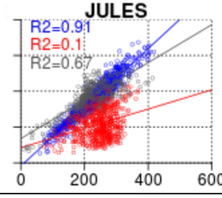

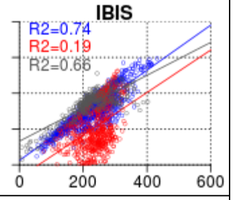

No soil model; (modified Priestley-Taylor)

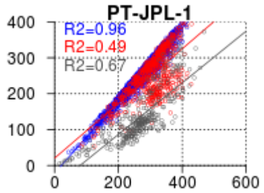

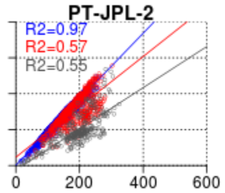

Shallow/ Intermediate, + aquifer

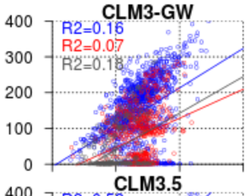

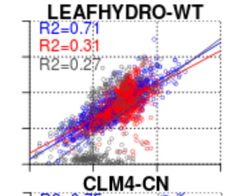

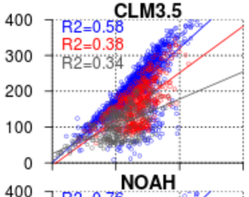

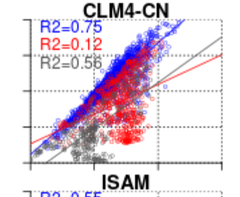

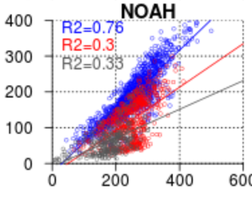

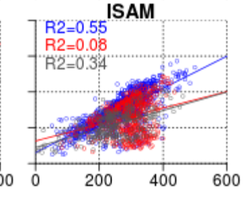

K34

Figure D1. Same as Figure 3 (main text), except for K34 site, and showing all participating models of the LBA-DMIP (de Gonçalves et al., in press), grouped by soil depth and presence/absence of an aquifer below the soil domain. Modeled components of E (E_s, E_i, E_t) shown in different shades of blue and components of total runoff Q_t (Q_s, Q_{sb}) shown as different oriented hashes (see legend).

Observations

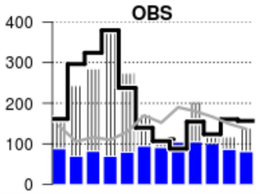

Shallow (< 3.5 m), no aquifer

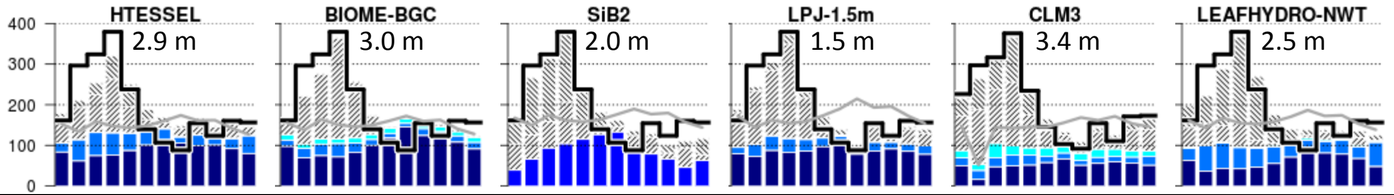

Intermediate (3.5 – 5.0 m), no aquifer

deep roots added

aquifer added

Deep (> 5m), no aquifer

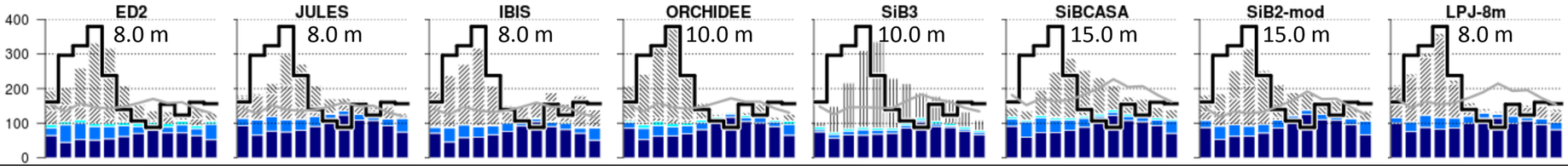

Energy Inputs:
R_n , net radiation (water equivalent)
Water Inputs:
P, precipitation
$P + Q_{g\uparrow}$, precipitation + groundwater flux (positive into system)
Water Outputs:
$Q_s + Q_{sb}$
Q_{sb}, subsurface drainage to streams & groundwater
Q_s , surface runoff
E , total evapotranspiration
E_s , soil evaporation
E_i , interception evaporation
E_t , transpiration
Soil Moisture Storage:
ΔS = ∑(water inputs) – ∑(water outputs),
change in soil moisture storage (difference between P (+ Qg, if any) and top of stacked bars)

No soil model; (modified Priestley-Taylor)

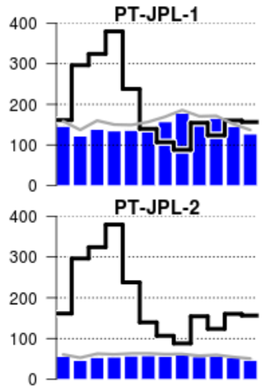

Shallow/ Intermediate, + aquifer

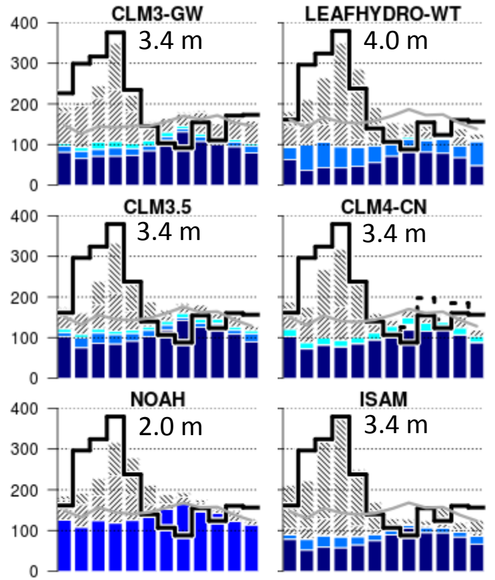

Figure D2. Same as Figure D1, except for K67 site.

K67

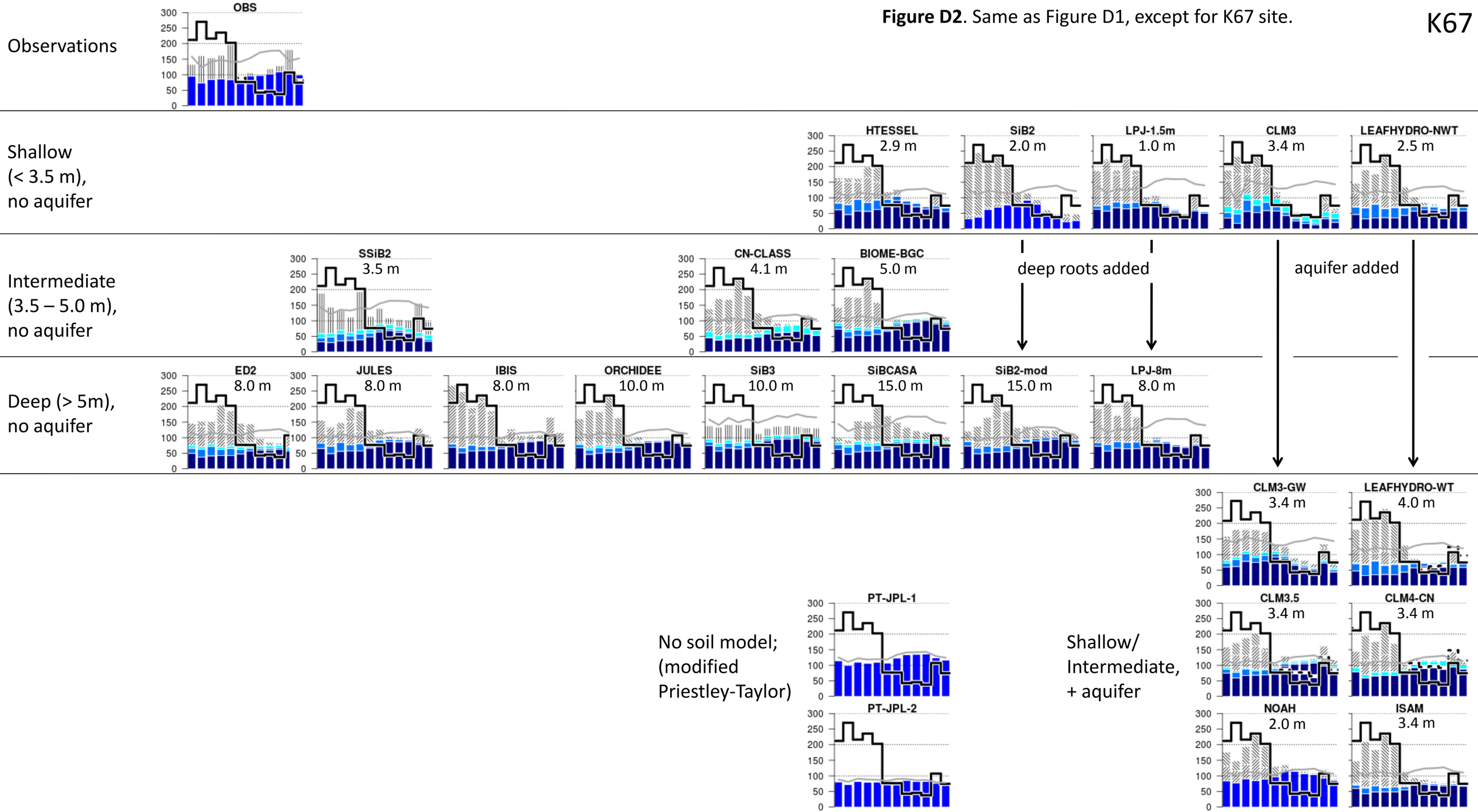

Figure D3. Same as Figure D1, except for K83 site.

K83

Observations

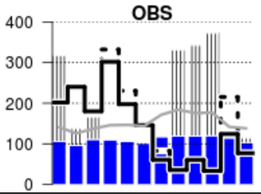

Shallow
(< 3.5 m),
no aquifer

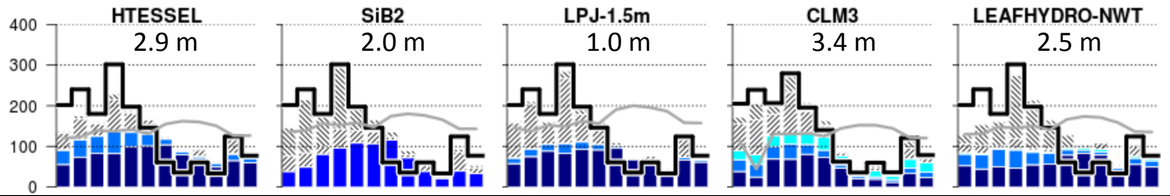

Intermediate
(3.5 – 5.0 m),
no aquifer

deep roots added

aquifer added

Deep (> 5m),
no aquifer

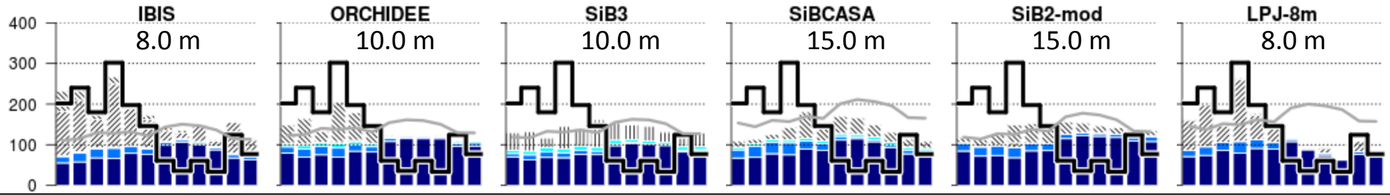

No soil model;
(modified
Priestley-Taylor)

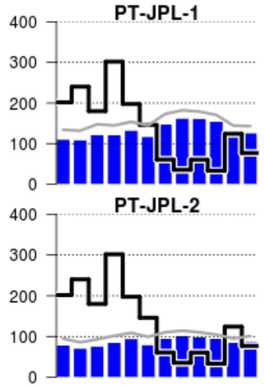

Shallow/
Intermediate,
+ aquifer

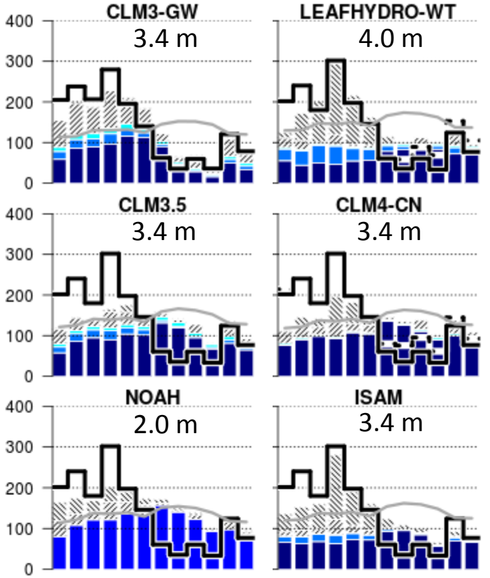

Figure D4. Same as Figure D1, except for RJA site.

RJA

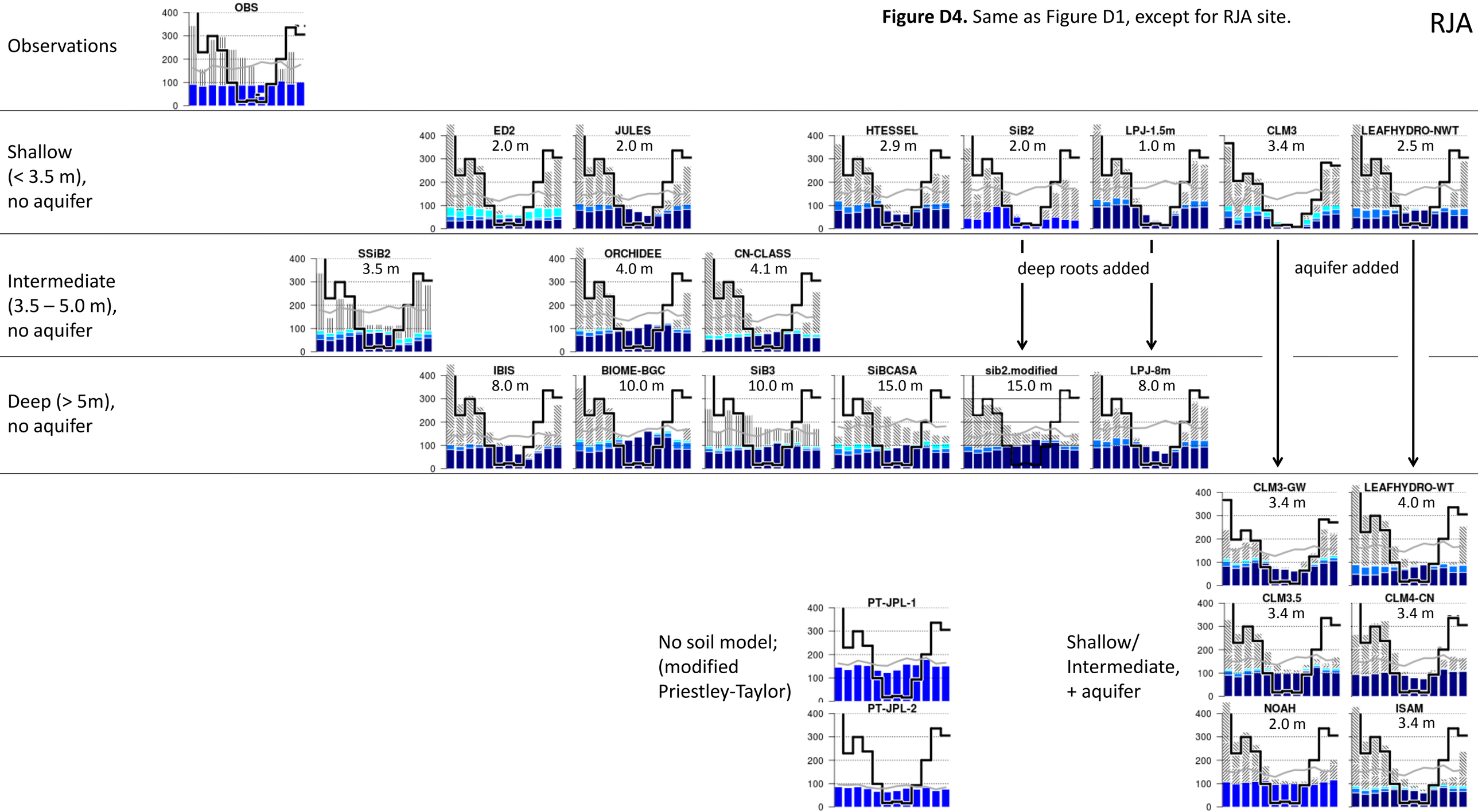

Figure D5. Same as Figure D1, except for BAN site.

BAN

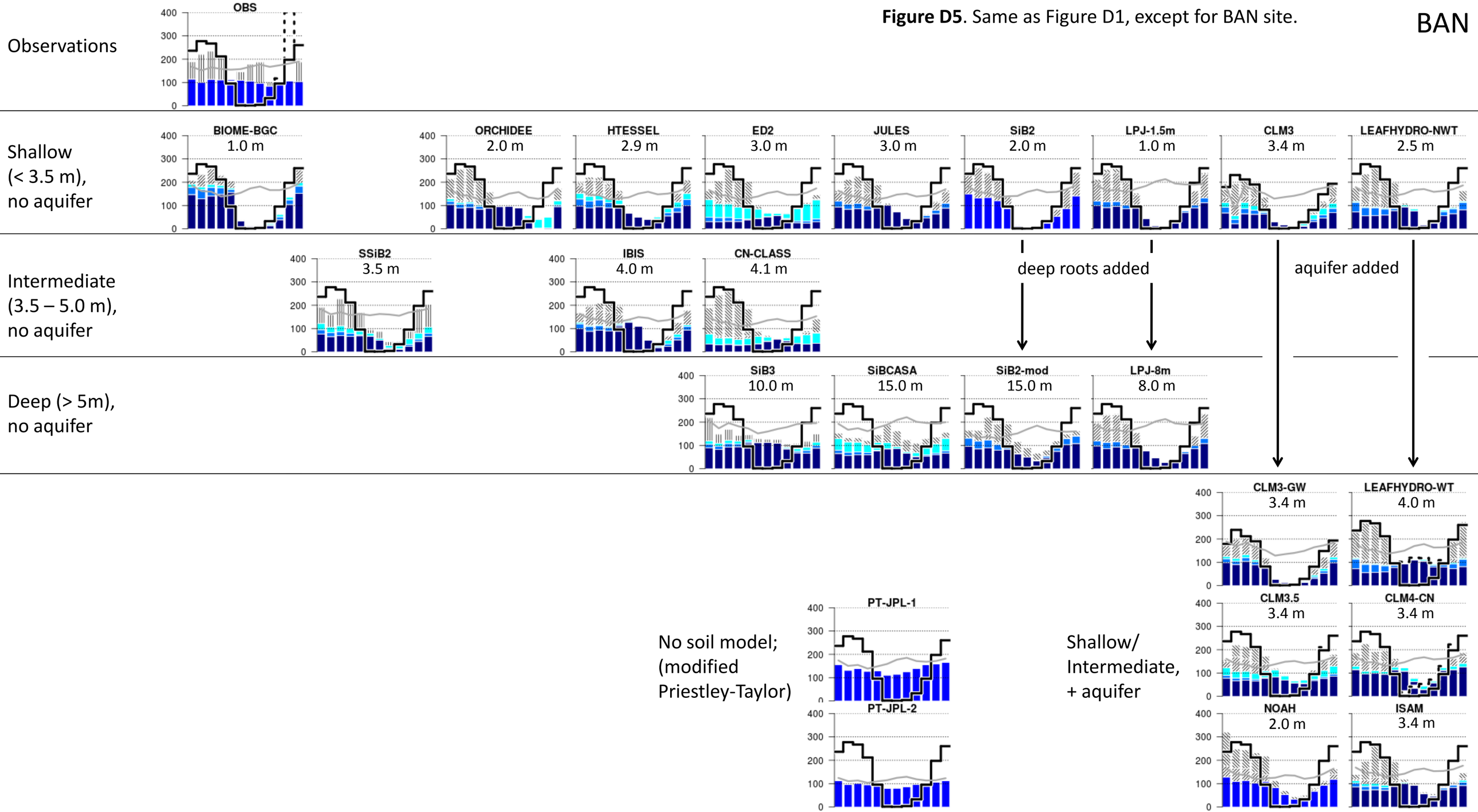

Figure D6. Same as Figure D1, except for PDG site.

PDG